Computer Simulation Studies of a Single Polyelectrolyte Chain in Poor Solvent

Alexey V. Lyulin[1,2], Burkhard Dünweg*[1],

Oleg V. Borisov[2], Anatoly A. Darinskii[2]

[1] Max–Planck–Institut für Polymerforschung,

Ackermannweg 10, D–55128 Mainz, Germany

[2] Institute of Macromolecular Compounds,

Russian Academy of Sciences,

199004 St.Petersburg, Russia

Abstract

The conformational behavior of a single, intrinsically flexible, weakly charged polyelectrolyte chain in poor solvent is analyzed by extensive computer simulations combining Monte Carlo and Molecular Dynamics techniques. After determining the Θ point for the charge–free case, we focus on the weak screening limit, corresponding to low salt concentration in the solution. We study the dependence on both the solvent strength, characterized by the relative deviation from the Θ point, τ, and the fraction of charged monomers in the chain, which is effectively tuned by varying the Coulomb interaction parameter. The conformations are discussed in terms of global properties (like the end–to–end distance, the inertia tensor components, etc.), and functions revealing more detailed information, like the density distribution around the center of mass, and the structure factor. For chains in the Θ regime our data confirm the picture of a string of electrostatic blobs. For poorer solvents (up to $\tau = 0.4$) we observe, upon increasing the intra–chain Coulomb repulsion, a splitting of the spherical globule into a dumbbell–type structure, accompanied by a sharp increase in the chain's gyration radius. For sufficiently large τ, a further splitting is observed as well. Such a "necklace globule" (a sequence of transitions) had been predicted by Dobrynin, Rubinstein and Obukhov (Macromolecules 1996, v. 29, p. 2974), with a nontrivial scaling of the gyration radius with chain length and interaction parameters, which is confirmed by our data. By means of a scaling analysis we argue that the transitions can be interpreted as thermodynamic first–order phase transformations, when taking the appropriate thermodynamic limit, which implies a scaling of the electrostatic coupling with inverse chain length.

1 Introduction

Polyelectrolytes represent a broad and very important class of materials including most biological[1,2] and many synthetic polymers. In the last few decades considerable progress has been achieved in the understanding of the behavior of polyelectrolytes in solution.[3,4] While many neutral polymers are not soluble in water, polyelectrolytes usually are, which is the main reason for their biological, and, increasingly, their technological importance. This solubility is caused by the presence of charged monomers and the large gain in translational entropy when counterions are released into the bulk of the solution. However, for uncharged monomers water is usually a very poor solvent, i. e. the interaction between uncharged monomers has the character of short–range attraction. If the fraction of uncharged monomers in the chain is sufficiently high (this is the case for weakly charged polyelectrolytes) this short–range attraction can induce a collapse transition (Θ transition), i. e. the formation of a polyelectrolyte globule. A particularly spectacular example of this marginal solubility in water is polystyrenesulphonate (PSS), where even a small fraction of non–sulphonated (and hence strongly hydrophobic) styrene monomer units is sufficient to cause the formation of intra– and inter–chain aggregates in dilute solution.[5,6]

The first theoretical model for the conformation of an individual weakly charged polyelectrolyte molecule in a poor solvent was proposed by Khokhlov.[7] This model suggested that, due to the balance between the electrostatic repulsion and the globule's surface tension, the chain forms an elongated cylinder (a "cigar"). However, the cylindrical globule is unstable with respect to capillary wave fluctuations, which cause a splitting into spherical collapsed cores and extended strings. The equilibrium intra–chain tension in the string is determined (up to finite size corrections) only by the solvent strength, i. e. by

the strength of the short–range attraction between the monomers. This instability was first shown for a neutral polymer subjected to an external extensional force in a poor solvent.[8,9] Later it was realized that it also occurs for charged chains, where the extension is caused by the intramolecular Coulomb repulsion.[10,11] The effect is analogous to the splitting of a charged liquid droplet into an array of smaller ones, which was predicted by Rayleigh long ago.[12] Because of the connectivity of the monomers one can expect the formation of a necklace type structure in which collapsed spherical beads are connected by extended narrow strings whose tension balances the Coulomb repulsion. This necklace model for the polyelectrolyte globule in a salt–free solution has recently been proposed by Dobrynin, Rubinstein and Obukhov (DRO).[11] It focuses on the essential features, which are short–range attraction (poor solvent condition) and long–range repulsion (unscreened Coulomb interactions in a salt–free solution) between monomers connected to a chain. Earlier such a necklace structure had been predicted by Kantor and Kardar[10] for a polyampholyte chain with an excess charge, which provides the long–range repulsion, while the short–range attraction is a result of correlations in the fluctuations of the intra–chain charge distribution. A very recent calculation on necklace formation was done by Solis and Olvera de la Cruz,[13] where the instability of the cylinder–like conformation was demonstrated by a variational approach.

The DRO necklace model can be considered as an alternative to the cylindrical model by Khokhlov. Both models predict a structure which is locally collapsed but strongly extended on large scales. However, in contrast to the homogeneous cylindrical model, the DRO model predicts a strong longitudinal modulation in the thickness of the extended polyelectrolyte globule. Because of the presence of long strings connecting the collapsed beads the overall longitudinal dimension of the chain is larger and, as a result, the energy

of the intra–chain Coulomb repulsion is smaller. Another major difference between the models is the nature of the conformational changes which the chain undergoes as either the Coulomb repulsion (i. e. the charge density) is increased, or the monomer–monomer attraction (i. e. the solvent strength) is decreased. While the Khokhlov model predicts a smooth deformation of the globule into a more and more elongated object, the DRO model implies a sequence of rather abrupt changes: The spherical globule splits into a dumbbell, the dumbbell into a trimbell, etc. These transitions can be considered as first–order phase transitions in the thermodynamic limit of infinite chain length, $N \to \infty$, while they are strongly smeared out for finite chains (as is the Θ collapse, which is however second–order in the thermodynamic limit). It should be noted that the long–range nature of the Coulomb interaction allows a well–defined thermodynamic limit only if, simultaneously with $N \to \infty$, the strength of this interaction tends to zero (for more details see below).

The experiments with PSS[5,6] provide some indications, but not a direct proof of the existence of the necklace polyelectrolyte globule. One of the main experimental difficulties is the necessity to work with very dilute solutions to prevent inter–chain aggregation. On the other hand, the very dilute regime is rather favorable for computer simulations (see, e. g., Ref. 14), since one can study a single chain, thereby avoiding most of the technical complications related to the long–range interactions with the periodic images of a simulation cell. However, rather long runs are necessary in order to obtain good statistics of the chain conformations, in particular in the transition regimes where fluctuations are large and relax slowly. Nevertheless, taking these caveats into account, computer simulations should be able to provide the most direct and least ambiguous proof of the correctness of the DRO picture. It is the purpose of the present paper to do this in more detail, and with better statistics, than the existing previous studies: Refs. 15

and 16 observed a sharp increase of the chain size with charge density, but did not analyze the conformations in more detail. The original DRO paper[11] presented Monte Carlo results of a chain consisting of up to 200 monomers. A similar sharp increase was observed; however, the main evidence for the correctness of the model was drawn from snapshots, while density distributions etc. were not studied systematically. Moreover, the Θ transition was not localized in this study, which is however important in order to quantify the notion of a poor solvent. In the present paper, we use extensive combined Monte Carlo (MC) and Molecular Dynamics (MD) simulations in order to systematically analyze the conformations of a weakly charged polyelectrolyte chain with short–range attraction between monomers, scanning a wide range of the phase diagram both with respect to degree of ionization and with respect to solvent quality, and paying particular attention to the transition from the spherically symmetrical globule to the extended state.

The present investigation is complementary to other simulations of the conformations of polyelectrolytes. We employ the same methodology as Ref. 17. That latter study, however, has rather studied a Θ chain with varying strength and range of the electrostatic interaction. In a realistic system, the concentration is always finite, which also means a finite concentration of counterions, implying some degree of electrostatic screening. The present simulation studies the case of an extremely large screening length, which, for practical purposes, can be viewed as an unscreened Coulomb interaction. This case may be somewhat unphysical compared to typical experimental systems (note that the dissociation of water makes it impossible to completely eliminate the counterions by dilution); however, it is the simplest case, and theoretically best understood. It is therefore even more interesting to note that both collapsed globules as well as DRO necklace globules also occur for more realistic systems. This has been shown in recent simulations of many–

chain systems with explicit counterions,[18,19] where it was also observed that the collapsed chains can form a rather dense fluid phase without precipitation, in close analogy to charge–stabilized colloids.

The paper is organized as follows: In Sec. 2 we review the main predictions of the scaling theories of a polyelectrolyte globule, and show how the formation of an additional bead on the necklace can be viewed as a first–order phase transition. Section 3 contains the description of the model and the simulation algorithm. In Sec. 4 we study the uncharged reference chain and determine its Θ point, while Sec. 5 presents our main results for the charged chain. Section 6 concludes with a brief discussion.

2 Theoretical Predictions

We start with a brief review of the main theoretical predictions concerning the behavior of a polyelectrolyte chain under poor solvent conditions. Both pertinent scaling theories[7,11] deal with weakly charged intrinsically flexible polyelectrolyte chains. The condition of intrinsic flexibility implies that the Kuhn segment length of the reference polymer chain (in the absence of charges) is of order of the chain thickness taken as a monomer unit length, b. The condition of weak charging can be formulated as a requirement of small fraction f of (elementary) charged monomer units in the chain, or, more specifically,

$$fu^2 \ll 1, \tag{2.1}$$

where $u = l_B/b$ is the dimensionless coupling parameter characterizing the strength of the Coulomb interactions and $l_B = e^2/(4\pi\epsilon k_B T)$ is the Bjerrum length (here e is the elementary charge, ϵ the dielectric constant of the solvent, k_B Boltzmann's constant and T the temperature). The condition of weak charging, Eqn. 2.1, implies that the Coulomb repul-

sion between neighboring charges (along the chain) is too weak to significantly perturb the Gaussian chain statistics between them — note that short–range repulsive excluded volume interactions play no role since we consider the system near its Θ point. The length scale on which the chain remains virtually unperturbed by intra–chain Coulomb repulsion and retains its Gaussian shape is called the electrostatic blob[20,21] and its size is equal to

$$\xi_e \cong b \left(f^2 u \right)^{-1/3} , \tag{2.2}$$

while the number of monomers in a blob is

$$g_e \cong \frac{\xi_e^2}{b^2} \cong \left(f^2 u \right)^{-2/3} . \tag{2.3}$$

If the condition of weak charging, Eqn. 2.1, is fulfilled, the number of charges per electrostatic blob, $f g_e = (f u^2)^{-1/3}$, is large. Therefore, the discrete character of the charge distribution does not play any role for the conformational properties of the chain on a scale comparable or larger than ξ_e. Hence a weakly charged polyelectrolyte chain with discrete charge distribution is equivalent to one with a smeared–out charge distribution, i. e. a fractional charge ef per monomer. The strength of the intra–chain Coulomb repulsion (normalized to $k_B T$) can be thus characterized by the dimensionless parameter $f^2 u$. On length scales above ξ_e, the Coulomb repulsion dominates and leads to a stretching of the chain (obviously, this can occur only for sufficiently long chains, $bN^{1/2} \gg \xi_e$, where N denotes the number of monomers). Envisioning the chain as a string of electrostatic blobs (in close analogy to Pincus blobs[22] for a chain which is stretched by external forces), one finds for the size of the chain (under Θ conditions)

$$R_\Theta \cong \frac{N}{g_e} \xi_e \cong \frac{N b^2}{\xi_e} \cong bN \left(f^2 u \right)^{1/3} . \tag{2.4}$$

Below the Θ point there is also a short–range attraction between the monomers, whose strength is characterized by the second virial coefficient between uncharged monomers.

This is proportional to the relative deviation from the Θ temperature, $\tau = (\Theta - T)/\Theta$; remember that the Θ temperature is defined for a chain *without* charges as the point at which it acquires Gaussian statistics. We hence consider an uncharged chain first. The pertinent length scale is the thermal correlation length or blob size[23]

$$\xi_t \cong \frac{b}{\tau}. \tag{2.5}$$

Below the scale of ξ_t, the attractive interactions are unimportant and the chain is Gaussian. One thermal blob contains

$$g_t \cong \frac{\xi_t^2}{b^2} \cong \tau^{-2} \tag{2.6}$$

monomers. Above ξ_t the structure is a collapsed globule, which, again, is of course only possible for sufficiently long chains, $bN^{1/2} \gg \xi_t$. For such a close–packed array of thermal blobs the overall size is

$$R_{gl} \cong \left(\frac{N}{g_t}\right)^{1/3} \xi_t \cong bN^{1/3}\tau^{-1/3}, \tag{2.7}$$

while the average monomer density is

$$\rho \cong \frac{g_t}{\xi_t^3} \cong \frac{\tau}{b^3}. \tag{2.8}$$

When both Coulomb repulsive and short–range attractive interactions are present, the dimensionless ratio ξ_e/ξ_t becomes a natural scaling variable. In the limit of dominant electrostatic interactions, corresponding to $\xi_e/\xi_t \ll 1$, the polyelectrolyte chain behaves as in a Θ solvent, i. e. its conformation is expected to be a string of electrostatic blobs described by Eqn. 2.4. In the opposite limit, where the short–range attraction is strong ($\xi_e/\xi_t \gg 1$), the chain is in a poor solvent, and its conformations are governed by the interplay between short–range attraction and long–range repulsion. The models of Khokhlov[7] and of DRO[11] are both concerned with that case, and both start from the assumption that in thermal

equilibrium the object is a densely packed array of thermal blobs of size ξ_t. However, it is no longer a spherical globule, but rather assumes an extended shape, thereby lowering its electrostatic energy F_e, while paying with an increase in surface energy F_s. It is the balance between those two terms which determines the equilibrium shape, and they are roughly estimated via

$$F_e \cong \frac{Q^2}{\epsilon L} \tag{2.9}$$

and

$$F_s \cong \frac{k_B T}{\xi_t^2} A, \tag{2.10}$$

where Q is the overall charge of the object, L its linear extension (in the long direction), and A its surface (each thermal blob at the surface contributes $k_B T$).

Khokhlov[7] assumed that the object is just an elongated cylinder. By minimization of the free energy with respect to its shape one finds that its thickness is just ξ_e, while its length is given by

$$R_{cyl} \cong bN\tau^{-1} \left(f^2 u\right)^{2/3}, \tag{2.11}$$

and the equilibrium free energy is

$$\frac{F}{k_B T} \cong \frac{Nb^2}{\xi_t \xi_e} \cong N\tau \left(f^2 u\right)^{1/3}. \tag{2.12}$$

The DRO picture,[11] on the contrary, assumes a necklace globule, i. e. a stretched–out sequence of thick spherical globules ("beads") connected by thin strings which are also elongated. The model allows for three variational parameters, which, e. g., can be chosen as the thicknesses of the beads and the strings, and the length of the strings. Since the model is treated in the long–chain limit, the number of beads is large and can be treated as a continuous parameter which just follows from the three lengths, the density, Eqn. 2.8, and the total number of monomers, N. Minimizing the free energy for such an object, one

finds that the equilibrium size of the beads is again given by ξ_e, which nicely corresponds to the cylinder thickness in the Khokhlov picture. The thickness of the string is ξ_t, which is as small as it can get without loosing excessive amounts of conformational entropy. Finally, the result for the length of the strings is

$$l_{str} \cong \xi_e \left(\frac{\xi_e}{\xi_t}\right)^{1/2} \cong b \left(\frac{\tau}{f^2 u}\right)^{1/2} \gg \xi_e. \tag{2.13}$$

Since the bead volume ξ_e^3 is much larger than the string volume $\xi_e^{3/2}\xi_t^{3/2}$, the beads contain practically all of the chain's mass. For that reason, the number of beads is simply given by

$$N_{bead} \cong \frac{N}{\rho \xi_e^3} \cong \frac{N f^2 u}{\tau}, \tag{2.14}$$

while for the length of the necklace globule one finds

$$R_{nec} \cong N_{bead} l_{str} \cong b N \tau^{-1/2} \left(f^2 u\right)^{1/2}. \tag{2.15}$$

Note that this implies a different scaling of R with the interaction parameters $f^2 u$ and τ than the Khokhlov picture, Eqn. 2.11. This different scaling, apart from the observation of abrupt changes in R, will allow us to test the Khokhlov prediction against the DRO picture.

For the DRO free energy in equilibrium finds the same formula as Eqn. 2.12, i. e. cylinder and necklace globule have, in leading order, the same scaling behavior of the free energy. However, the necklace globule has a smaller prefactor, as is demonstrated in more detail in Appendix A (the wording of Ref. 11 on this issue may be somewhat misleading to some readers). The leading–order contributions to the free energy are the intra–bead repulsion (i. e. the Coulombic self–energy of a bead, disregarding the interaction with the other beads), and the bead surface energy, which balance each other; both contributions

are of order $k_B T N b^2/(\xi_e \xi_t)$ (where we have summed over all beads). The inter–bead repulsion is of order $k_B T N b^2/(\xi_e^{3/2} \xi_t^{1/2})$ (the intra–string repulsion is negligible); it is balanced by the string energy, which is of same order. It is important to notice that these contributions are much smaller than the leading–order terms (by a factor of $(\xi_t/\xi_e)^{1/2}$). This is the reason why in leading order the Coulombic bead–bead interactions may be neglected, such that in essence the old Rayleigh[12] picture applies. It should however also be noticed that this is only correct as long as the number of beads does not become too large — otherwise logarithmic contributions from the bead–bead interactions become important (these have been neglected in the DRO treatment[11]).

A transition in the DRO picture is just the increase of N_{bead} by one. From this, one sees that the natural scaling variable, which determines the effective strength of the electrostatic interaction, is $N f^2 u/\tau$. Moreover, this also shows how the thermodynamic limit has to be taken properly for the present system: If we would consider the system just as a function of $f^2 u$, then an infinitely long chain would jump from a globule ($f^2 u = 0$) into an infinitely long stretched–out state with infinitely many beads at infinitesimally weak repulsion, i. e. all transitions would just "collapse" into one single transition at $f^2 u = 0$. If, however, one considers the limit $N \to \infty$, $f^2 u \to 0$, $N f^2 u = \text{const.}$, then the number of beads remains constant, i. e. the beads and strings simply get bigger and bigger without any instability. Furthermore, by rewriting Eqn. 2.12 as

$$\frac{F}{k_B T} \cong N^{2/3} \tau^{4/3} \left(\frac{N f^2 u}{\tau} \right)^{1/3} , \tag{2.16}$$

one sees that the free energy scales as $N^{2/3}$, i. e. in the considered limit one must view quantities which scale as $N^{2/3}$ as thermodynamically extensive quantities.

Three final remarks are still necessary. Firstly, upon increasing the strength of the

electrostatic repulsion, the number of beads progressively increases, while their size ξ_e decreases. At very large f^2u the interaction is so strong that the condition $\xi_e \gg \xi_t$ no longer holds. One then enters the regime of a Θ solvent, where the chain extension is rather described by Eqn. 2.4. This is however a smooth crossover: At the crossover point $\xi_e = \xi_t$ or $f^2u = \tau^3$, the chain extension of the necklace globule (Eqn. 2.15) coincides with that of the string of electrostatic blobs (Eqn. 2.4). At this point the Khokhlov cylinder (Eqn. 2.11) has also the same length.

Secondly, the above derivation has explicitly exploited the large–N limit, i. e. the possibility to treat N_{bead} as a continuous variable. However, this limit is not accessible to simulations, due to limitations in computer power. Moreover, the limit of small N_{bead}, i. e. the transition globule $\rightarrow$ dumbbell $\rightarrow$ trimbell etc., is also physically more interesting, since here the changes in the chain's shape are much more pronounced. Therefore, we have analyzed the transition globule $\rightarrow$ dumbbell in some more detail. Obviously, the globule's geometry is completely fixed by its spherical shape and the density, while for the dumbbell we have one variational parameter, e. g. the bead size, assuming a string thickness of ξ_t at the outset. This results in a nontrivial optimization problem, which however can be solved in the asymptotic limit $N \rightarrow \infty$, $f^2u \rightarrow 0$, $Nf^2u = \text{const.}$. Sorting the resulting terms according to the powers of N, one sees that one has to balance the string length against the overall repulsion, resulting in contributions to the free energy $\propto N^{1/2}$, while the leading order terms are proportional to $N^{2/3}$, describing the balance between intra–bead repulsion and bead surface tension. Since in the considered limit the mass fraction in the string is negligible, the bead size is simply determined by splitting the mass between the two beads. It therefore turns out that the scaling formulae of the DRO model (in particular Eqn. 2.15) do also hold in the limit of small N_{bead}. Since R

according to Eqn. 2.15 depends on N, f^2u, and τ in the same way for each of the necklace states, one must expect that the transition from the globule to the dumbbell is far more pronounced than all the other transitions.

Thirdly, it is not immediately obvious in what sense the transition $N_{bead} \to N_{bead} + 1$ can be viewed as a thermodynamic phase transition. In order to answer this question, we make the following observations: If an interpretation as a phase transition is justified, then we must view Nf^2u/τ (or, for constant τ, more conveniently Nf^2u) as the "field" which drives the transition. The corresponding thermodynamically conjugate variable, normalized as an intensive variable (which for simplicity we call the order parameter m), then must be subject to a singularity at the transition (jump in case of a first–order transition, infinite slope in case of a second–order transition). This can however be explicitly checked for the DRO picture by noting that the order parameter is

$$m = -N^{-2/3} \frac{\partial F}{\partial (Nf^2u)}, \tag{2.17}$$

by definition of the thermodynamic conjugate, taking into account that the scaling of the free energy F with chain length, Eqn. 2.16, implies a normalization with $N^{-2/3}$. Now, in a model with fractional charge ef on each monomer, the Hamiltonian can be written as

$$\mathcal{H} = \mathcal{H}_0 + \frac{k_BT}{2} f^2 u \sum_{i \neq j} \frac{b}{r_{ij}}, \tag{2.18}$$

where $\mathcal{H}_0$ contains all the non–electrostatic terms, while $\vec{r}_{ij} = \vec{r}_i - \vec{r}_j$, $\vec{r}_i$ denoting the position of monomer i. From

$$F = -k_BT \ln \int d^3\vec{r}_1 \ldots \int d^3\vec{r}_N \exp\left(-\mathcal{H}/\left(k_BT\right)\right) \tag{2.19}$$

one can directly evaluate the derivative in Eqn. 2.17, resulting in

$$m = -k_BT \frac{bN^{1/3}}{2R_H} \tag{2.20}$$

with

$$\frac{1}{R_H} = \frac{1}{N^2} \sum_{i \neq j} \left\langle \frac{1}{r_{ij}} \right\rangle . \tag{2.21}$$

R_H is usually called the hydrodynamic radius of the chain.[24] We did not sample this quantity in our simulations because we had not yet realized its significance at the production stage of our work. For a DRO necklace globule with N_{bead} beads of size d_{bead}, the behavior of R_H may be estimated by the following reasoning (which is quite analogous to that in Ref. 11): First, we exploit the fact that the beads contain practically all the mass. For that reason we may assume that the monomers i and j which contribute to the sum in Eqn. 2.21 are actually bead monomers — the fraction of interactions which involve string monomers is tiny. Within one bead, there are (N/N_{bead}) monomers, and hence the number of interactions within that bead is $(1/2)(N/N_{bead})^2$. A typical value for r_{ij} within the bead is d_{bead}, and hence the contribution from one bead is estimated as $(N/N_{bead})^2/d_{bead}$. For a given pair of beads, the number of interactions is (up to a factor of 2) the same; however, here each interaction contributes only with $1/l_{str}$, which is much smaller. For this reason, we may also neglect the bead–bead interactions, unless the number of beads is quite large, giving rise to many of these interactions. These latter contributions are however logarithmic contributions, which are also consistently neglected in the DRO treatment.[11] We hence find by summing up the intra–bead contributions

$$\frac{1}{R_H} \cong \frac{1}{N^2} N_{bead} \left(\frac{N}{N_{bead}} \right)^2 \frac{1}{d_{bead}} = \frac{1}{N_{bead} d_{bead}}. \tag{2.22}$$

From this one sees that R_H for the present system has a somewhat different meaning than for neutral polymer coils. While for the coil R_H is just another measure of the chain extension, such that the ratio R/R_H is a universal number, we here find for that ratio

$$\frac{R}{R_H} \cong \frac{l_{str}}{d_{bead}} \cong \left(\frac{\xi_e}{\xi_t} \right)^{1/2}, \tag{2.23}$$

by using $d_{bead} \cong \xi_e$, and Eqn. 2.13. The ratio therefore strongly depends on the interaction. The order parameter m can be interpreted as the ratio of the single–globule size (cf. Eqn. 2.7; note that τ must be considered a constant) to the total size of all the beads in the DRO necklace. Furthermore, from Eqns. 2.2 and 2.14 one finds

$$m \cong -k_B T \tau^{1/3} N_{bead}^{-2/3}, \tag{2.24}$$

i. e. the order parameter jumps whenever a new bead is added. This means that the transition $N_{bead} \rightarrow N_{bead} + 1$ is indeed a thermodynamic first–order phase transition. Moreover, the magnitude of these jumps decreases more and more as N_{bead} increases, i. e. the transitions get weaker and weaker.

Figure 1 summarizes the DRO picture in terms of a schematic phase diagram in the (double–logarithmic) $(\tau, f^2 u)$ plane. In regions I_Θ and I_- the chain is so weakly charged that it is in essence unperturbed by the Coulomb repulsion. Region I_Θ corresponds to the Gaussian coil, while in region I_- the chain has a globule conformation. In region II_Θ the chain is represented by a linear sequence of electrostatic Gaussian blobs. Region II_- corresponds to the necklace globule described above. The lines $\tau \sim u f^2 N$, $\sim u f^2 N/2$, $\sim u f^2 N/3, \ldots$, mark the phase boundaries between the single spherical globule, the dumbbell, the three–bead necklace, etc.

3 Model and Simulation Method

We consider a freely jointed uniformly charged chain consisting of N monomers. The non–electrostatic interactions between all the monomers are described by the modified

Lennard–Jones potential

$$U_{LJ}^{(m)}(r) = \begin{cases} 4\epsilon_{LJ}\left\{\left[\left(\frac{\sigma}{r}\right)^{12} - \left(\frac{\sigma}{r}\right)^{6} + \frac{1}{4}\right] + \beta\left[\cos\frac{2\pi r}{r_c} - 1\right]\right\}, & r < r_c \\ 0, & r > r_c \end{cases} \tag{3.1}$$

with $r_c = 2^{1/6}\sigma$. This potential (see Fig. 2) introduces a very narrow attractive part such that the range of interaction remains short. The strength of the attractive interaction is varied via the parameter β; this is equivalent to varying the solvent strength. We use σ as a unit of length, ϵ_{LJ} as a unit of energy and the monomer mass, m, as a unit of mass. All further quantities will be presented in this unit system. The calculations were performed at temperature $k_BT = 1.0$.

The bonds between neighboring monomers are described by the finitely extendable nonlinear elastic (FENE) potential

$$U_{FENE}(r) = -\frac{k}{2}r_0^2 \ln\left(1 - \frac{r^2}{r_0^2}\right), \tag{3.2}$$

where k is a spring constant and r_0 the maximum bond length. The simulation was performed with the standard parameters $k = 30$ and $r_0 = 1.5$[25,26] which keep the bond length at a nearly constant value $b \approx 1$.

All monomers interact with each other (in addition to the short–range Lennard–Jones potential, Eqn. 3.1) via a screened Coulomb (Debye–Hückel) potential:

$$\frac{U_C(r)}{k_BT} = l_B\frac{\exp\left(-r/l_D\right)}{r}, \tag{3.3}$$

where l_B is the Bjerrum length (see Sec. 2) and l_D the Debye length which describes the screening of the electrostatic interactions due to the presence of counterions and salt in the solution. At very low concentration of both salt and polyelectrolyte this screening effect becomes negligible, i. e. l_D becomes much larger than the extension of even a stretched

chain, and the interaction becomes effectively purely Coulombic. It is this limit which we have studied in the present work, using a value of $l_D = 500$, while our longest chain is made of $N = 256$ monomers.

In our simulation we varied the strength of the intra–chain Coulomb repulsion via the Bjerrum length l_B, from which we calculated the dimensionless interaction parameter $u = l_B/b$, using the bond length we actually sampled in the simulation. At constant temperature this can correspond to a change in the solvent dielectric constant, or to a change in the fraction of charged monomers in the chain, or both. As outlined in more detail at the beginning of Sec. 2, the overall charge may be distributed homogeneously on the chain, without altering the essential physics. Hence in our model the parameter f^2u of Sec. 2 has to be replaced by just u, which was varied from $u = 0$ (neutral chain) up to $u \approx 1$. It turned out that most interesting effects occur in this regime. Moreover, above $u \cong 1$ one expects Manning counterion condensation[27] to occur in a realistic system (unless the concentrations are extremely small): The Coulomb interaction becomes so strong that entropy is no longer able to keep all counterions in solution. Of course, this effect cannot be described within our model, since the counterion degrees of freedom are not present.

It should be noticed that, strictly spoken, we would have to restrict the range of u even much further, in order for the theory of Sec. 2 to fully apply. The problem is that for large u (of order unity) we violate the condition of weak charging, as is seen from Eqn. 2.1, setting $f = 1$. This simply means that for the larger values of u our model, which is based on a fractional charge on each monomer, is not fully equivalent to the same chain with full charges on the corresponding fraction of monomers. All other predictions of the theory remain valid. The reason why we had to introduce this deficiency is a purely technical

one: In order to get into the regime of the globule $\rightarrow$ dumbbell transition at small u, one would have to work with very long chains, as seen from Eqn. 2.14. This is however computationally very hard, for reasons of long equilibration times. Other simulations like Ref. 17 have faced similar problems to reach the limit of weak charging.

The ensemble–averaged chain properties were obtained by a hybrid Monte Carlo algorithm in close analogy to the procedure employed in Ref. 17. In order to achieve efficient sampling (i. e. short correlation times) on both long and short length scales, we combined an off–lattice pivot algorithm[28] with stochastic dynamics, i. e. MD coupled to a Langevin heat bath via friction and noise,[25] using a damping constant $\gamma = 1.0$. The equations of motion were solved by the velocity Verlet integrator[29] with a time step $h = 8 \times 10^{-3} \ldots 10 \times 10^{-3}$ in units of the natural Lennard–Jones time $t_{LJ} = \sigma \left(m/\epsilon_{LJ}\right)^{1/2}$. In order to ensure that data were taken from sufficiently long runs, we started the simulations from two very different configurations, a fully stretched chain and a coiled conformation which was generated by placing a self–avoiding random walk on a cubic lattice. We then required that both runs, within statistical accuracy, would produce identical results. Without such a test procedure it is very hard to reliably check that the simulation data are actually valid equilibrium values. In particular, we tested the end–to–end distance R,

$$\left\langle \vec{R}^2 \right\rangle = \left\langle (\vec{r}_N - \vec{r}_1)^2 \right\rangle , \tag{3.4}$$

the gyration radius R_g,

$$\left\langle R_g^2 \right\rangle = N^{-1} \sum_{i=1}^{N} \left\langle \left(\vec{r}_i - \vec{R}_{cm} \right)^2 \right\rangle \tag{3.5}$$

(with $\vec{R}_{cm}$ the chain's center of mass), and the bond length b. Before taking data, the chains were equilibrated by repeating the following hybrid procedure between three and eight times (depending on chain length and solvent quality): First the local structure

was equilibrated by 10^5 MD steps, and then the overall structure was relaxed by adding 5×10^4 pivot moves. In the subsequent production stage MD and MC were more thoroughly mixed: After $20 \ldots 50$ MD steps we added one pivot move, and repeated this procedure until we had collected $1 \times 10^7 \ldots 3 \times 10^7$ steps in total. The acceptance rate for the pivot moves varied between roughly 10% for neutral chains and $30\% \ldots 50\%$ for the largest values of u. In all cases, we observed a systematic increase of the acceptance rate with increasing chain stretching. In order to estimate the number of generated statistically independent chain conformations we calculated the normalized time autocorrelation function of the squared end–to–end distance

$$C_{R^2}(t) = \frac{\langle R^2(0) R^2(t) \rangle - \langle R^2 \rangle^2}{\langle R^4 \rangle - \langle R^2 \rangle^2} \tag{3.6}$$

and obtained the correlation time t_R from $C_{R^2}(t_R) = e^{-1}$. The number of independent conformations is then given by the ratio $n_{conf} = t_{run}/(2t_R)$, where t_{run} is the length of the overall run.[30] In all simulations the statistics was satisfactory, $n_{conf} = 100 \ldots 1000$.

Several conformational characteristics were evaluated. During every production run 2000 measurements were done. Aside from R and R_g (see Eqns. 3.4 and 3.5) we also studied the inertia tensor[31,32]

$$T^{cm}_{\alpha\beta} = \frac{1}{N} \sum_{i=1}^{N} x_{i\alpha} x_{i\beta}, \tag{3.7}$$

where $x_{i\alpha}$ and $x_{i\beta}$ are the α and β cartesian components of $\vec{r}_i - \vec{R}_{cm}$. At each measurement we calculated the eigenvalues λ_i of T^{cm}, ordered them according to their size (such that $\lambda_1 \geq \lambda_2 \geq \lambda_3$), and averaged them afterwards, thereby removing the trivial rotational symmetry which otherwise would produce identical values. The roots of these eigenvalues are measures of the chain dimensions along the three orthogonal principal axes.

Furthermore we calculated the probability distribution function $P(R)$ of the end–to–

end distance and the spherically averaged monomer density $\rho(r)$ in the chain's center–of–mass reference frame. The latter function was used in Ref. 33 to characterize the internal structure of a partially ionized polyelectrolyte chain consisting of hard spheres. In our calculation the distances were divided into intervals of size $\Delta = N/500$ and a frequency count for each stroboscopic configuration was done. The distribution functions were normalized so that the area under the distribution curve equals unity.

Finally, we also analyzed the chain conformations by the single–chain structure factor

$$S(q) = \frac{1}{N} \sum_{ij} \langle \exp\left(-i\vec{q}(\vec{r}_i - \vec{r}_j)\right) \rangle \,. \tag{3.8}$$

As was calculated in Ref. 11, one expects

$$\begin{aligned} S(q) \;\approx\; & \frac{m_{bead}^2}{N} \left(N_{bead} + 2 \sum_{k=1}^{N_{bead}-1} (N_{bead} - k) \, \frac{\sin(q l_{str} k)}{q l_{str} k} \right) \\ & \left(\frac{\sin(q d_{bead}) - q d_{bead} \cos(q d_{bead})}{(q d_{bead})^3} \right)^2 \end{aligned} \tag{3.9}$$

for a DRO necklace globule with N_{bead} beads of size d_{bead}, each of which contains m_{bead} monomers, and which are separated by strings of length l_{str}.

4 Results for Neutral Chains: Θ Point and Globular State

In order to determine the β region (cf. Eqn. 3.1) corresponding to poor solvent conditions for our model polyelectrolyte chain, it is necessary to determine first the value of β_Θ which corresponds to the Θ point for the uncharged chain ($u = 0$). At $\beta = \beta_\Theta$ the short–range attractive interactions between monomers compensate their excluded volume and the chain without charges becomes Gaussian, $R^2 \cong Nb^2$. For $\beta < \beta_\Theta$, corresponding to good

solvent conditions, the chain is a swollen coil, $R^2 \sim N^{2\nu} b^2$ ($\nu \approx 0.59$), while in the poor solvent region $\beta > \beta_\Theta$ the chain collapses into a globule, $R^2 \sim N^{2/3} b^2$.

This collapse transition was studied by simulating neutral chains of length $N = 5, 9, 17, 33, 65, 129$. In Fig. 3 we plot $\langle R^2 \rangle / (N b^2)$ vs. N^{-1} for different values β. At $\beta = \beta_\Theta$ the N–dependence must flatten off for large N. From this we find $\beta_\Theta = 2.53 \pm 0.1$. An analogous procedure was used, e. g., in Refs. 34, 35 and 36.

As a consistency check, we also tested the scaling relation[35–38]

$$\frac{\langle R^2 \rangle}{N b^2} = f(\tau N^{1/2}), \tag{4.1}$$

where τ is the normalized distance from the Θ point,

$$\tau = \frac{\beta - \beta_\Theta}{\beta_\Theta}, \tag{4.2}$$

and $f(x)$ is a universal scaling function with the asymptotic behavior[23]

$$f(x) \propto \begin{cases} |x|^{4\nu - 2}, & x \ll -1 \\ x^0, & |x| \ll 1 \\ x^{-2/3}, & x \gg 1. \end{cases} \tag{4.3}$$

This is done in Fig. 4, where one sees that the curves for various chain lengths nicely collapse when using the scaling argument $\tau N^{1/2}$. This is a further indication for having found the correct value β_Θ. However, the data do not reach far into the good solvent and poor solvent regimes, such that the asymptotics indicated in Eqn. 4.3 is not visible.

For the ratio $\langle R^2 \rangle / \langle R_g^2 \rangle$ at $\beta = \beta_\Theta$ we found a value close to 6, as it should be for a Gaussian chain. The calculated ratio $\langle \lambda_1 \rangle^{1/2} : \langle \lambda_2 \rangle^{1/2} : \langle \lambda_3 \rangle^{1/2} = 3.43 : 1.63 : 1$ agrees also very well with the ratio $3.44 : 1.64 : 1$ for a random walk.[31]

Further data at $u = 0$ were taken deeper in the poor solvent regime, where one expects

for the gyration radius (see Eqn. 2.7)

$$\frac{\left\langle R_g^2 \right\rangle^{1/2}}{bN^{1/3}} = k\tau^{-1/3}. \tag{4.4}$$

This relation is tested in Fig. 5 for chain length $N = 129$; we find good agreement in the region $0.02 < \tau < 0.2$ with a proportionality constant $k = 0.27$. For longer chains, one expects the globular regime to extend to even smaller values of τ, corresponding to the values of the scaling variable $N^{1/2}\tau \gg 1$.

At larger τ the dependence of $\langle R_g^2 \rangle^{1/2}$ on τ deviates from the theoretically predicted one given by Eqn. 2.7. The reason is simply that for strong attraction the monomers become effectively close–packed, such that no further shrinking is possible. The deviation becomes significant at $\tau \approx 0.2$, which corresponds to the gyration radius $R_g \approx 2.3$. However, for a spherical globule of radius R_{tot} with uniform density, $R_g = (3/5)^{1/2} R_{tot}$. Hence the globule's radius is estimated as $R_{tot} = 3.0$, corresponding to a density of $\rho = 0.85$. This is a very high density at which typically simulations of polymer melts are performed.[26]

5 Results for Charged Chains

In the charged case $u > 0$ we have studied only chains of $N = 129$ and $N = 256$ monomers. We varied τ from 0 up to 0.39 and u from 0 to 0.6, thus scanning a wide range of solvent strength (under poor solvent conditions) and of degree of ionization.

When the electrostatic interactions are switched on, the size and the shape of the chain start to change. Figure 6 summarizes how the gyration radius (normalized by Nb) increases as a function of u. One clearly sees that quite different behavior occurs for different solvent strengths τ. For vanishing or small τ one observes the scaling predicted by Eqn. 2.4, thus confirming the picture of a string of electrostatic blobs[20] in the Θ regime.

None of the other formulae considered in Sec. 2 predicts a $u^{1/3}$ behavior. A similar result for a charged chain near Θ was obtained in Ref. 16. In the poor solvent regime (typically for $\tau > 0.1$, which corresponds well to the $N^{1/2}\tau \gg 1$ criterion) the curves look quite different, but also cross over into the same $u^{1/3}$ behavior for large u. This indicates that for such large electrostatic repulsion the solvent becomes a Θ solvent again, in perfect agreement with the scaling theory which says that effectively Θ conditions are present when $\xi_e \ll \xi_t$ or $u \gg \tau^3$. The data also support the theoretical prediction that this change in behavior is a smooth crossover (this is also true for all the other data we produced in that regime, as will be seen below). Moreover, one sees that in the large–u limit the gyration radius becomes practically independent of τ, again in agreement with Eqn. 2.4.

For smaller u the behavior is however quite different: For very small u the gyration radius remains essentially unaffected by the Coulomb repulsion, while it sharply increases at larger u. This qualitative observation is in better agreement with the DRO picture than with Khokhlov's. Interpreting the sharp increase as the formation of a necklace out of the globule, one expects an $u^{1/2}$ increase of R_g in the necklace phase (see Eqn. 2.15), while for a cylinder one would get $u^{2/3}$ behavior (Eqn. 2.11). As is seen in Fig. 6, DRO behavior is indeed visible; however, it is practically impossible to distinguish it from $u^{2/3}$, due to the overall rounding of the curves.

A clearer understanding is obtained when replotting the data according to the various scaling predictions, as is done in Fig. 7. Firstly, one sees that the location of the sharp increase is roughly the same if one uses the scaling variable Nu/τ instead of u, as predicted by the DRO picture. The transition is located at $uN/\tau \approx 25$. Secondly, we normalize R_g in such a way that it is a constant according to the various predictions: For single–globule scaling, we plot $R_g\tau^{1/3}/(bN^{1/3})$ (Eqn. 2.7), for necklace scaling $R_g\tau^{1/2}/(Nbu^{1/2})$ (Eqn.

2.15), and for Khokhlov scaling $R_g\tau/(Nbu^{2/3})$ (Eqn. 2.11). Indeed, if one disregards the data for $\tau < 0.1$ (which are still in the Θ regime), one sees that the DRO predictions are confirmed in the respective phases (globular scaling below the transition, necklace scaling above), while Khokhlov scaling is not confirmed (instead of being constant, the data exhibit a continuous decrease). When τ is varied at constant u, the same behavior is observed, which is of course far from surprising (data not shown).

Further indications of the strong stretching at $Nu/\tau \approx 25$ come from the parameters $r = \langle R^2\rangle/\langle R_g^2\rangle$ (Fig. 8) and the "asphericity" factor[39]

$$\Delta = \frac{3\left\langle \sum_i (\lambda_i - \overline{\lambda})^2 \right\rangle}{2\left\langle \left(\sum_i \lambda_i\right)^2 \right\rangle} \tag{5.1}$$

with $\overline{\lambda} = (\lambda_1 + \lambda_2 + \lambda_3)/3$. Data for Δ are not shown; the curves look rather similar to those of Fig. 8, varying between zero and one. As before, we use Nu/τ as appropriate scaling variable. For a spherical globule, $\Delta = 0$, while $r = 2$ if the chain ends are distributed randomly over the globule's volume. However, for entropic reasons the chain ends are expected to be preferentially located at the globule's surface, in which case $r = 10/3$. Further known values are $r = 6$ and $\Delta = 10/19$[39] for a Gaussian chain, and $r = 12$ and $\Delta = 1$ for a completely stretched chain. Similarly to the behavior of R_g, one finds smooth stretching near Θ (small τ), while for larger τ both r and Δ increase sharply at the transition $Nu/\tau \approx 25$. Both parameters show that even for the strongest repulsion the chain has not yet reached its fully stretched state. Moreover, the value of $r \approx 3$ in the globular state confirms the picture of chain ends located at the surface.

Since the observed chain stretching is only incomplete, the fluctuations in the end–to–end distance are quite large, even for the most extended conformations. This is demonstrated in quite some detail in Fig. 9, where we plot the probability distribution of the

end–to–end distance, $P(R)$, for various values of τ and u. Near the Θ point (small τ) one observes a unimodal distribution whose maximum is shifted to larger R as the electrostatic repulsion is increased, consistent with the picture of continuous stretching of a Θ chain. At larger τ, however, we observe that the distribution gets much narrower for $u = 0$, corresponding to the globule, while at intermediate values of u a *bimodal* distribution is found. We interpret this bimodal distribution as phase coexistence between globule and dumbbell; a criterion for the location of the first–order transition is the requirement that both peaks have the same statistical weight.[40] Actually, from looking at Fig. 9, one would locate the transition at $\tau = 0.24, u \approx 0.05$ and $\tau = 0.29, u \approx 0.06$, corresponding to $Nu/\tau \approx 25$ for both cases ($N = 129$), in perfect agreement with the previous analysis. Figure 10 studies $P(R)$ of the $N = 129$ chain at constant electrostatic repulsion $u = 0.05$ for increasing τ. The stretched Θ chain is smoothly transformed into a necklace globule without any particular changes in $P(R)$, while again the bimodal distribution at $\tau = 0.24, u = 0.05$ indicates phase coexistence with the globule, which remains the only stable phase for even larger τ. It should be mentioned that $P(R)$ in the globular state will look different for different chain end locations (bulk of the globule vs. surface); however, our data are not accurate enough to see this difference clearly. Hence it turns out that the value $\langle R^2 \rangle / \left\langle R_g^2 \right\rangle \approx 3$ is a better indicator for the chain end localization at the surface.

The stretching is also associated with a strong peak in the specific heat (Fig. 11), evaluated via the fluctuation relation

$$C_v = \frac{1}{N(k_B T)^2} \left(\left\langle U^2 \right\rangle - \langle U \rangle^2 \right), \tag{5.2}$$

where U is the overall potential energy. Such a strong peak is quite typical for a phase transition; again for all systems it occurs at the same location $Nu/\tau \approx 25$. For the

poorest solvent $\tau = 0.39$ the peak is rather broad and also somewhat shifted to larger values of Nu/τ. We believe that the reason for this is the formation of the trimbell phase, a transition which is not well separated from the globule $\rightarrow$ dumbbell transition within our limitations of resolution and chain length. Looking back at Fig. 6, one sees for $\tau = 0.39$ a weak shoulder in R after the initial sharp increase; this might also be related to this transition (note that the theory expects the change in R to be much more dramatic for the globule $\rightarrow$ dumbbell transition than for dumbbell $\rightarrow$ trimbell).

Nevertheless, these indications are very weak, and one would like to analyze the conformations within the necklace regime in more detail using more local information. To this end, we sampled the density distribution $\rho(r)$ of monomers around the chain's center of mass, presented in Fig. 12 for different values of τ and $N = 129$. It should be noted that for these plots we simply counted the monomers in a distance r from the center of mass, without taking geometric factors into account; this is the reason why ρ always tends to zero for $r \rightarrow 0$. The curves were normalized such that their area is unity.

At small τ, one simply observes a broadening of the distribution upon increase of the electrostatic interaction, corresponding to the stretching of the Θ chain. For $\tau = 0.24$, the behavior is however much more complex: First the narrow distribution corresponding to the globule becomes broader, then a bimodal distribution is observed, which can again be interpreted as phase coexistence between globule and dumbbell (phase transition at $u \approx 0.05$, same as above), followed by a unimodal density with a peak at large r which can be interpreted as a dumbbell. This distribution however becomes bimodal again for even larger u, corresponding to accumulation of mass near the center, or trimbell formation. In essence, the same behavior also occurs for the larger values of τ. We therefore conclude that the simulation indeed observes the trimbell phase.

In terms of the single–chain structure factor, which is shown in Fig. 13 for various τ and u and $N = 129$, the behavior is again simple for small τ: At the Θ point $\tau = 0$, $u = 0$ one nicely observes the q^{-2} scattering law of a Gaussian chain, while the stretched Θ chain ($\tau = 0$, large u) shows the expected q^{-1} decay. The Θ chain also shows that the oscillations starting approximately for $q > 5$ are associated with the molecular structure on the monomer level. For larger τ, $S(q)$ becomes more complicated. For $u = 0$ (globule) there are oscillations between $q = 1$ and $q = 5$, as expected for a sphere (see Fig. 14, where $S(q)$ is shown for some simple geometric structures). For larger u, there is an additional shoulder–like structure well below $q = 1$; this is associated with the additional length scale of the string in the necklace. Indeed, as is seen from Fig. 14, such a behavior is expected for a dumbbell, but not for a cylinder. The double shoulder which appears for $\tau = 0.39$, $u = 0.15$, is probably due to a trimbell structure or even more complicated conformations.

The most direct way to see the DRO necklace is of course the inspection of snapshot conformations, of which we present a few at the end of this section for the $N = 129$ chain in the poorest solvent $\tau = 0.39$ (Fig. 15). The sequence globule $\rightarrow$ dumbbell $\rightarrow$ trimbell occurring upon increasing the electrostatic repulsion is quite easily seen. Further increase of u extends the chain to such large dimensions that the (perhaps existing) stability of a further four–bead phase is strongly blurred.

6 Conclusions

As a result of our simulations we have obtained a detailed description of the conformations of a single, flexible polyelectrolyte chain in poor solvent. The conformational

transitions related to the collapse of the polyelectrolyte chain and induced by varying either the solvent strength (the relative deviation from the Θ point, τ) or the strength of the electrostatic interaction (coupling parameter $u = l_B/b$) have been analyzed. Apart from verifying the picture of a string of electrostatic blobs in the Θ regime, our data provide reliable evidence for the existence of the DRO[11] necklace type conformation of a polyelectrolyte chain under poor solvent conditions. Conversely, the older Khokhlov[7] picture of an extended cylinder is clearly ruled out, as is known since DRO's analytical and numerical work, and further corroborated in detail by our data: The scaling behavior for the chain extension is well consistent with the DRO picture, but not with Khokhlov's prediction. There is a well–defined transition in the chain size, also visible in the specific heat, which occurs at constant Nu/τ, as predicted by DRO. Further detailed analysis of the chain conformations (density distributions, structure factor, snapshots) revealed that not only the dumbbell phase, but also the trimbell structure was accessible within the parameter range of our simulation. A simulation which would attempt to observe even more beads unambiguously would involve substantially longer chains and a very large numerical effort.

All in all, the validity of the DRO picture is not too surprising, since it was already known since Rayleigh's times[12] that a large charged droplet is instable. However, the added understanding is that chain connectivity does not alter the picture — it is energetically and entropically possible to form strings between the beads which are sufficiently long and thin, such that the beads effectively do not interact, as in the old Rayleigh picture.

The characteristic features of the transition from the globule to the dumbbell are (i) a sharp change of the size and the shape of the chain, (ii) coexistence of two states in

the transition region and (iii) a peak in the specific heat. While this is quite typical for first–order phase coexistence, our scaling analysis has actually shown that this concept is well justified. As the nature of the transitions is now well understood, one can continue and study them with even higher accuracy, using reweighting and finite size scaling techniques.[40]

Nevertheless, some details of the phase diagram are still far from clear. The lines shown in Fig. 1 are, strictly spoken, lines which mark the crossovers between various regimes of the phase diagram. They are not true phase boundary lines, since the diagram is drawn for finite chain length, where all phase transitions are smeared out. In the thermodynamic limit $N \to \infty$, where phase transitions do exist, one can consider two cases: Either one studies an electrostatic interaction which tends to zero as $N \to \infty$, such that $Nf^2u = \text{const.}$, and the phase diagram is drawn in the (Nf^2u, τ) plane. In that case one has well–separated first–order transition lines between the necklace globule phases, which all end in the Θ point $Nf^2u = 0, \tau = 0$. In this phase diagram the Θ region has shrunken to the line $\tau = 0$. The alternative case is to leave all interaction parameters constant as $N \to \infty$, and draw the phase diagram in the (f^2u, τ) plane. Then all the transitions between the necklace globule phases shrink to a single transition at $f^2u = 0$, where the system jumps from the single globule to an extended necklace globule state (with infinitely many beads). The Θ region of this phase diagram occupies the area characterized by $\tau < \text{const.}(f^2u)^{1/3}$; in this region one has a string of electrostatic blobs, while for larger τ one enters the necklace globule phase. Our data indicate that this change is a smooth crossover, but do by no means exclude the possibility that it is actually a weak thermodynamic second–order phase transition. The order parameter of this transition would be the modulation in the thickness at a finite wavelength. The

amplitude of this modulation can become arbitrarily small, and would vanish in the Θ phase. Such a scenario is actually predicted by recent variational calculations.[13] A test by computer simulation has not been done yet; an attempt to provide an unambiguous proof would probably turn out to be rather difficult, and require both substantial computational efforts and advanced data analysis.

Acknowledgments

This study was supported by collaboration grant No. I/72164 from the Volkswagen foundation, and by RFFR grant No. 96-03-33833. Stimulating discussions with K. Kremer are gratefully acknowledged. Moreover, we thank U. Micka for letting us use his computer program, upon which ours was built.

A Rayleigh Instability

We here show in some more detail why a sufficiently large charged droplet should split into smaller ones,[12] and why this state is lower in energy than an elongated Khokhlov cylinder. In contrast to the scaling arguments of Sec. 2, we also take the prefactors into account.

Instead of a simple cylinder it is more convenient to consider a prolate ellipsoid with one large semi–axis a, and two identical small semi–axes b. Its volume is $V = (4\pi/3)ab^2$, while the surface area is given by $A = 4\pi ab$. It is useful to introduce the aspect ratio $x = a/b \geq 1$; a spherical droplet corresponds to the limiting case $x \to 1$. If the ellipsoid is charged with a homogeneous charge density ρ, such that the total charge is $Q = \rho V$,

then the electrostatic self–energy is given by[41]

$$U_{cyl,el} = \frac{3}{5}\frac{Q^2}{4\pi\epsilon a} f(x) \tag{A.1}$$

with

$$f(x) = \frac{\cosh^{-1} x}{\sqrt{1 - x^{-2}}}, \tag{A.2}$$

which increases monotonously with the aspect ratio x, starting at the value $f(x = 1) = 1$. We simplify the discussion by replacing the function f, which varies rather smoothly, by a constant f_0. Taking also the surface energy with surface tension σ into account, the total energy of the ellipsoid within this approximation is

$$U^{appr}_{cyl,tot}(f_0) = \frac{3 f_0}{5}\frac{Q^2}{4\pi\epsilon a} + \sigma\sqrt{12\pi a V}, \tag{A.3}$$

where the surface area has been expressed in terms of the parameters a and V. Optimizing this expression with respect to a at constant volume, and re–expressing the charge in terms of volume and charge density, one obtains

$$a = \frac{1}{4\pi}\left(\frac{12 f_0^2}{25}\right)^{1/3}\left(\frac{\rho^2}{\epsilon\sigma}\right)^{2/3} V \tag{A.4}$$

and

$$U^{appr}_{cyl,opt}(f_0) = 3\left(\frac{9 f_0}{20}\right)^{1/3}\left(\frac{\rho^2\sigma^2}{\epsilon}\right)^{1/3} V. \tag{A.5}$$

This provides a reasonable approximation to the energy of the ellipsoid when choosing a reasonable value for f_0. For example, for an aspect ratio of 10 one obtains $f(x = 10) = 3.008$. On a more rigorous basis, one can exploit the relation

$$U_{cyl,tot} > U^{appr}_{cyl,tot}(f_0 = 1), \tag{A.6}$$

which the true total energy satisfies. Taking the minimum value on both sides of the inequality, one sees that the true equilibrium energy of the ellipsoid is at any rate larger

than $U^{appr}_{cyl,opt}(f_0 = 1)$. As will be shown below, this latter energy is however precisely the value which is obtained for a set of spherical droplets of equal size ("Rayleigh state"), whose number is chosen to minimize the energy, and which are far enough away from each other to not interact (see discussion in Sec. 2 why this interaction can be neglected for the DRO necklace globule). It is hence shown that the preferred Rayleigh state differs from the cylinder by a smaller prefactor, up to corrections to scaling, which manifest themselves in the fact that $f(x)$ is, strictly spoken, not a constant.

Let us now discuss the Rayleigh state in some more detail. The energy of a spherical droplet is obtained from the above formulae by setting $x = 1$. When charge and size are expressed in terms of the volume, it is given by

$$U_{sph,tot} = \left(\frac{3}{4\pi}\right)^{2/3} \left[\frac{1}{5}\frac{\rho^2}{\epsilon}V^{5/3} + 4\pi\sigma V^{2/3}\right]. \tag{A.7}$$

If the volume is distributed onto *two* non–interacting droplets of volume V_1 and $V - V_1$ ($V_1 \leq V/2$), the energy is

$$U_{2,tot} = \left(\frac{3}{4\pi}\right)^{2/3} \left[\frac{1}{5}\frac{\rho^2}{\epsilon}\left(V_1^{5/3} + (V - V_1)^{5/3}\right) + 4\pi\sigma\left(V_1^{2/3} + (V - V_1)^{2/3}\right)\right]. \tag{A.8}$$

For small V and / or large $\sigma\epsilon/\rho^2$, this function is minimized for $V_1 = 0$, i. e. the one–droplet state. For sufficiently large V and / or small $\sigma\epsilon/\rho^2$, the minimum occurs at $V_1 = V/2$, i. e. the symmetric two–droplet state. Obviously, more and more splitting will occur when V is increased.

Suppose now that the volume has been distributed onto N droplets, where N is the optimum number of droplets. If, for a given pair of droplets, the sizes were different, the system could lower its energy by re–distributing the volume such that the pair is symmetric. Hence all droplets must have the same size in equilibrium. For this system

the energy is

$$U_{N,tot} = \left(\frac{3}{4\pi}\right)^{2/3} \left[\frac{1}{5}\frac{\rho^2}{\epsilon} N \left(\frac{V}{N}\right)^{5/3} + 4\pi\sigma N \left(\frac{V}{N}\right)^{2/3}\right]. \tag{A.9}$$

In the thermodynamic limit (V large, N large) N can be treated as continuous variable. Optimizing the above expression with respect to N yields for the size of a single droplet

$$\frac{V}{N} = \frac{15}{2}\frac{4\pi}{3}\frac{\epsilon\sigma}{\rho^2}, \tag{A.10}$$

while for the total energy in equilibrium one obtains exactly the same value as Eqn. A.5, evaluated at $f_0 = 1$, as anticipated above.

References

1. Lehninger, A. L. *Biochemistry;* Worth Publishers: New York, 1979.

2. Eisenberg, H. *Biological Macromolecules and Polyelectrolytes in Solution;* Clarendon Press: Oxford, 1976.

3. Oosawa, F. *Polyelectrolytes;* Dekker: New York, 1971.

4. Barrat, J.-L.; Joanny, J.-F. *Adv. Chem. Phys.* **1996,** *94,* 1.

5. Williams, C. E.; Wafa, E. *J. Phys. II* **1995,** *5,* 1269.

6. Wafa, E. *Structure des Polyelectrolytes Fortement Charges*, Ph. D. thesis, Universite Paris VI, 1996.

7. Khokhlov, A. R. *J. Phys. A* **1980,** *13,* 979.

8. Halperin, A.; Zhulina, E. B. *Europhys. Lett.* **1991,** *15,* 417.

9. Halperin, A.; Zhulina, E. B. *Macromolecules* **1991,** *24,* 5393.

10. Kantor, Y.; Kardar, M. *Europhys. Lett.* **1994,** *27,* 643.

11. Dobrynin, A. V.; Rubinstein, M.; Obukhov, S. P. *Macromolecules* **1996,** *29,* 2974.

12. Rayleigh, L. *Philos. Mag.* **1882,** *14,* 184.

13. Solis, F. J.; de la Cruz, M. O. *Macromolecules* **1998,** *31,* 5502.

14. Dünweg, B.; Stevens, M.; Kremer, K. in *Monte Carlo and Molecular Dynamics Simulation in Polymer Science*, edited by K. Binder, Clarendon Press: Oxford, 1995.

15. Hooper, H. H.; Beltran, S.; Sassi, A. P.; Blanch, H. W.; Prausnitz, J. M. *J. Chem. Phys.* **1990,** *93,* 2715.

16. Higgs, P. G.; Orland, H. *J. Chem. Phys.* **1991,** *95,* 4506.

17. Micka, U.; Kremer, K. *Phys. Rev. E* **1996,** *54,* 2653.

18. Micka, U.; Kremer, K. preprint, submitted to Phys. Rev. Lett.

19. Micka, U.; Holm, C.; Kremer, K. preprint, submitted to Langmuir.

20. de Gennes, P. G.; Pincus, P.; Velasco, R. M.; Brochard, F. *J. Phys. France* **1976,** *37,* 1461.

21. Khokhlov, A. R.; Khachaturian, K. A. *Polymer* **1982,** *23,* 1742.

22. Pincus, P. *Macromolecules* **1976,** *9,* 386.

23. de Gennes, P. G. *Scaling Concepts in Polymer Physics;* Cornell University Press: Ithaca, 1979.

24. Doi, M.; Edwards, S. F. *The Theory of Polymer Dynamics;* Clarendon Press: Oxford, 1986.

25. Grest, G. S.; Kremer, K. *Phys. Rev. A* **1986,** *33,* 3628.

26. Kremer, K.; Grest, G. S. *J. Chem. Phys.* **1990,** *92,* 5057.

27. Manning, G. S. *J. Chem. Phys.* **1969,** *51,* 924.

28. Sokal, A. D. in *Monte Carlo and Molecular Dynamics Simulation in Polymer Science*, edited by K. Binder, Clarendon Press: Oxford, 1995.

29. Allen, M. P.; Tildesley, D. J. *Computer Simulation of Liquids;* Clarendon Press: Oxford, 1987.

30. Müller-Krumbhaar, H.; Binder, K. *J. Stat. Phys.* **1973,** *8,* 1.

31. Solc, K.; Stockmayer, W. H. *J. Chem. Phys.* **1971,** *54,* 2756.

32. Ceperley, D.; Kalos, M. H.; Lebowitz, J. L. *Macromolecules* **1981,** *14,* 1472.

33. Christos, G. A.; Carnie, S. L. *J. Chem. Phys.* **1989,** *91,* 439.

34. Grest, G. S.; Murat, M. *Macromolecules* **1993,** *26,* 3108.

35. Milchev, A.; Paul, W.; Binder, K. *J. Chem. Phys.* **1993,** *99,* 2592.

36. Destree, M.; Lyulin, A.; Ryckaert, J.-P. *Macromolecules* **1996,** *29,* 1721.

37. Lai, P. Y.; Binder, K. *J. Chem. Phys.* **1992,** *97,* 586.

38. Kremer, K. in *Computer Simulation in Chemical Physics*, edited by M. P. Allen and D. J. Tildesley, Kluwer: Dordrecht, 1993.

39. Bishop, M.; Michels, J. P. J. *J. Chem. Phys.* **1986,** *85,* 5961.

40. Dünweg, B. in *Monte Carlo and Molecular Dynamics of Condensed Matter Systems*, edited by K. Binder and G. Ciccotti, Societa Italiana di Fisica: Bologna, 1996.

41. Wendt, G. in *Encyclopedia of Physics*, Vol. 26, edited by S. Flügge, Springer–Verlag: Berlin, 1958.

Figures

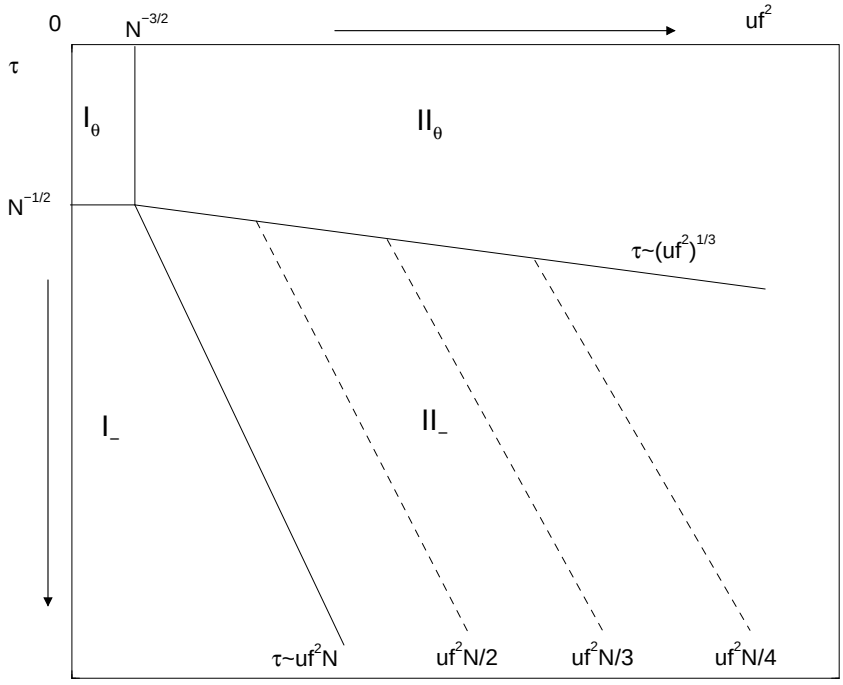

Figure 1: Phase diagram of a polyelectrolyte chain of N monomers in a poor solvent. $\tau = (\Theta - T)/\Theta$ measures the strength of the monomer–monomer attraction, while $u = l_B/b$, the normalized Bjerrum length, and f, the charge fraction, measure the strength of the Coulombic repulsion. Regime I_Θ corresponds to the unperturbed Gaussian coil, II_θ to the stretched chain of Gaussian blobs. In regime I_- the chain forms a globule, while in regime II_- a cascade of transitions to necklace globules is expected.

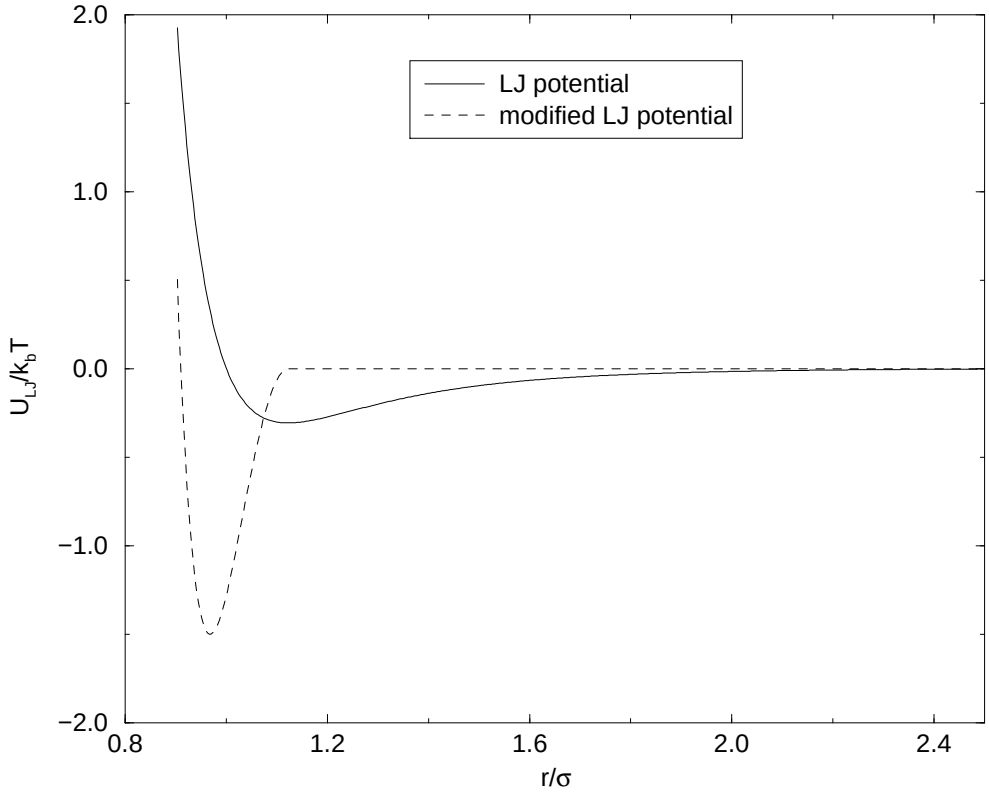

Figure 2: Nonbonded monomer–monomer potential, normalized by k_BT. Dashed line: Potential used in this work, see Eqn. 3.1, at $\epsilon_{LJ}/(k_BT) = 1$ and $\beta = 2.53$. As shown in Sec. 4, this corresponds to Θ conditions. Solid line, for comparison: Standard Lennard–Jones potential at $\epsilon_{LJ}/(k_BT) = 0.31$. According to Ref. 34, and consistent with exploratory test runs by us, this is again close to the Θ point of the corresponding system.

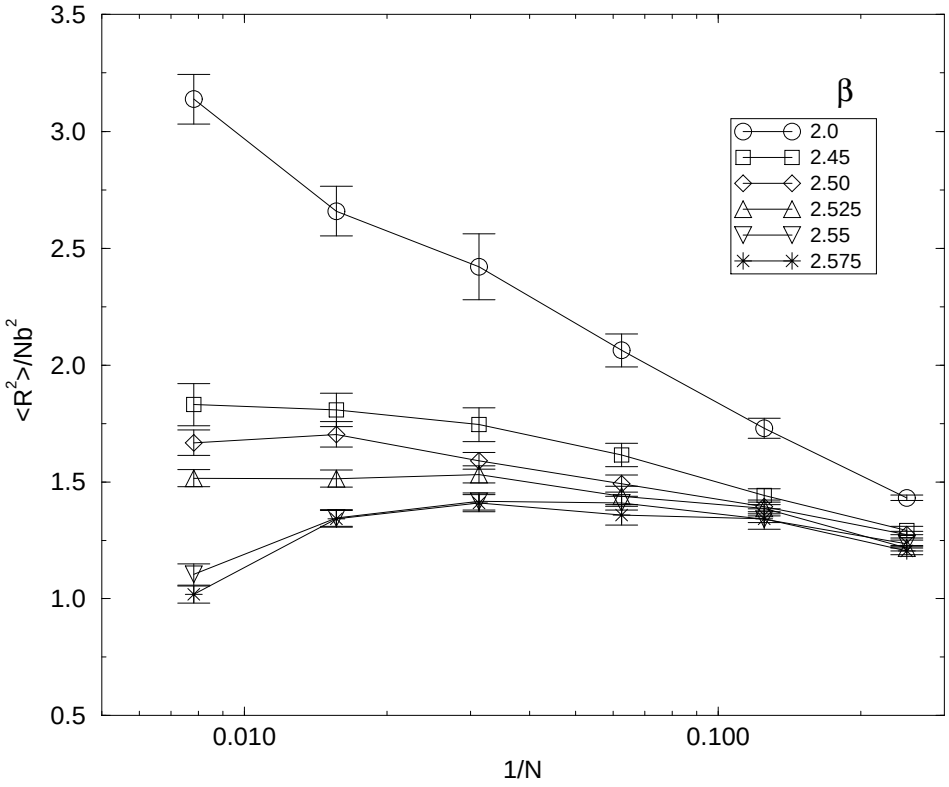

Figure 3: Chain length dependence of the normalized square of the end–to–end distance of a neutral chain, for different values of the parameter β of the modified Lennard–Jones potential.

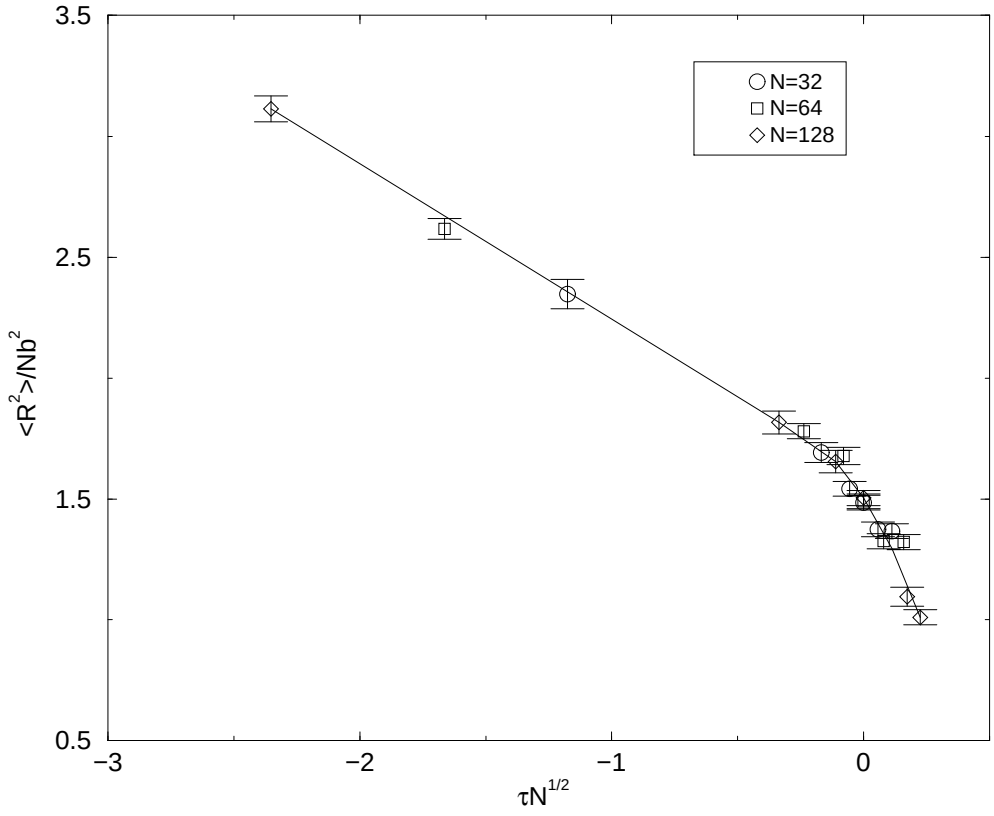

Figure 4: Universal behavior of the normalized square of the end–to–end distance of a neutral chain versus $\tau N^{1/2}$ for different chain lengths. The continuous line is a polynomial fit to the data as a guide to the eye.

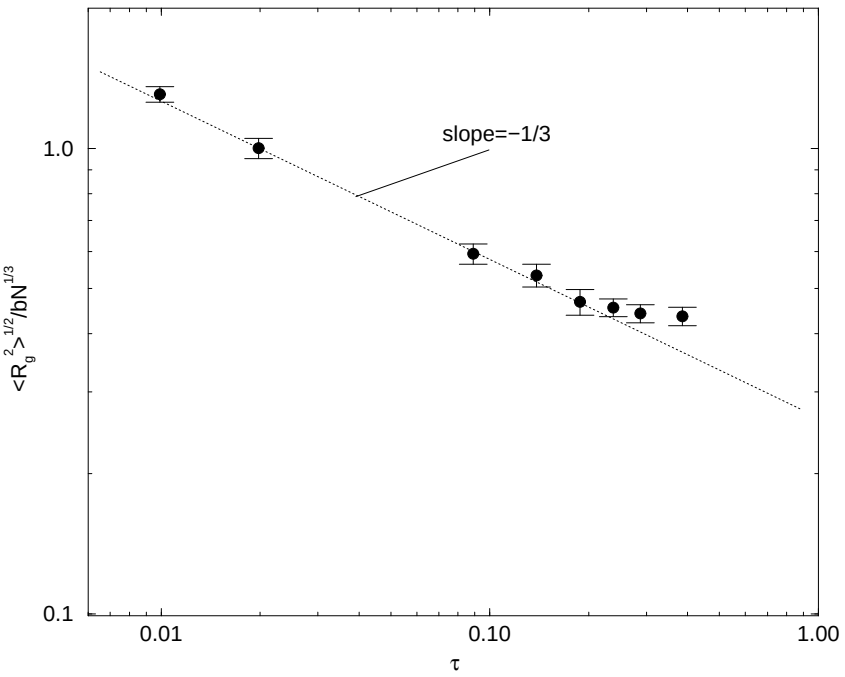

Figure 5: τ–dependence of the normalized radius of gyration of a neutral chain of $N = 129$ monomers in the globular state. The dashed straight line has a slope of $-1/3$.

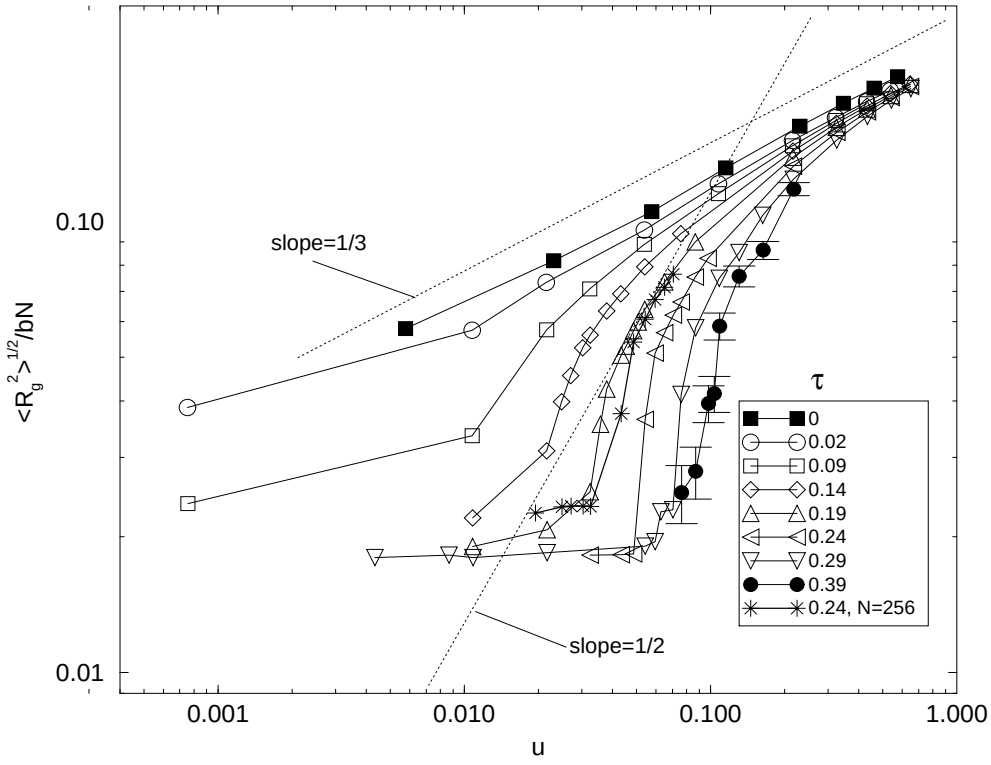

Figure 6: Dependence of the normalized gyration radius on the normalized Bjerrum length for different values of τ. All data are for $N = 129$ except one curve as indicated.

(a)

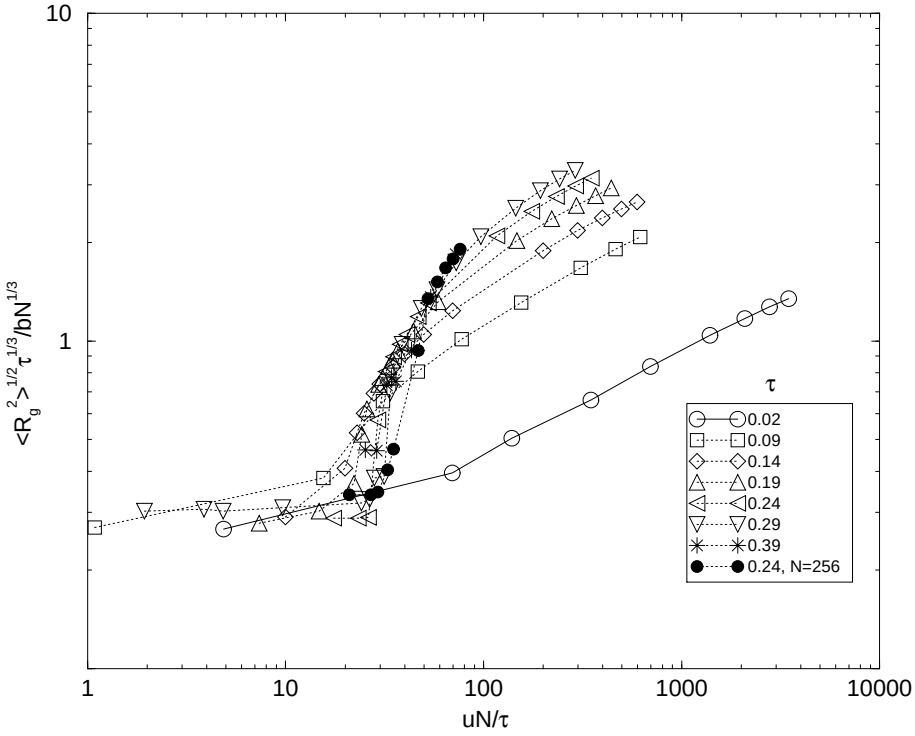

(b)

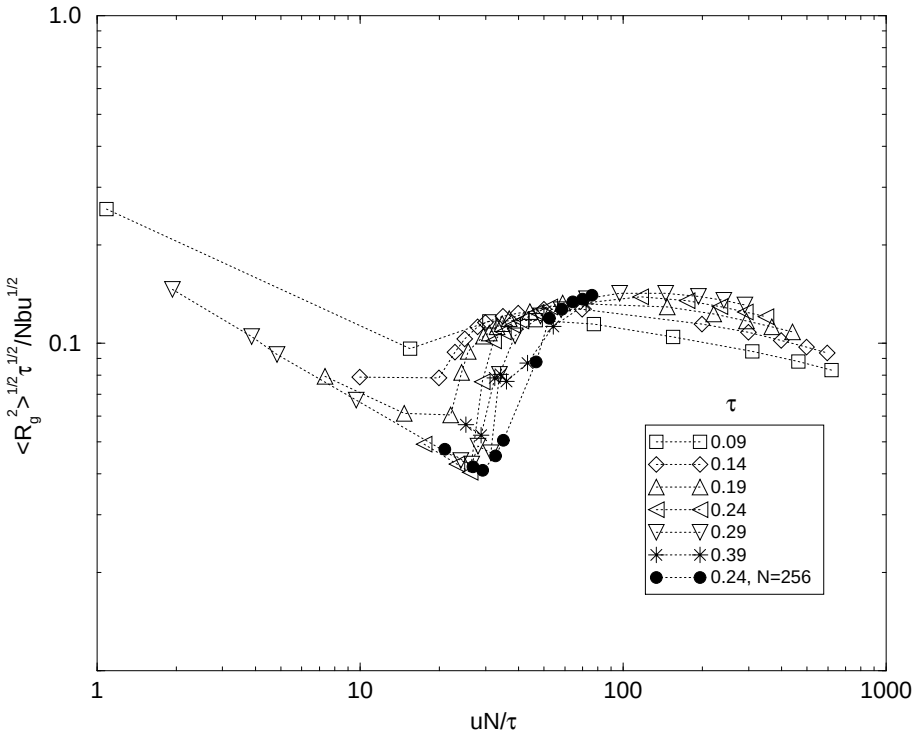

(c)

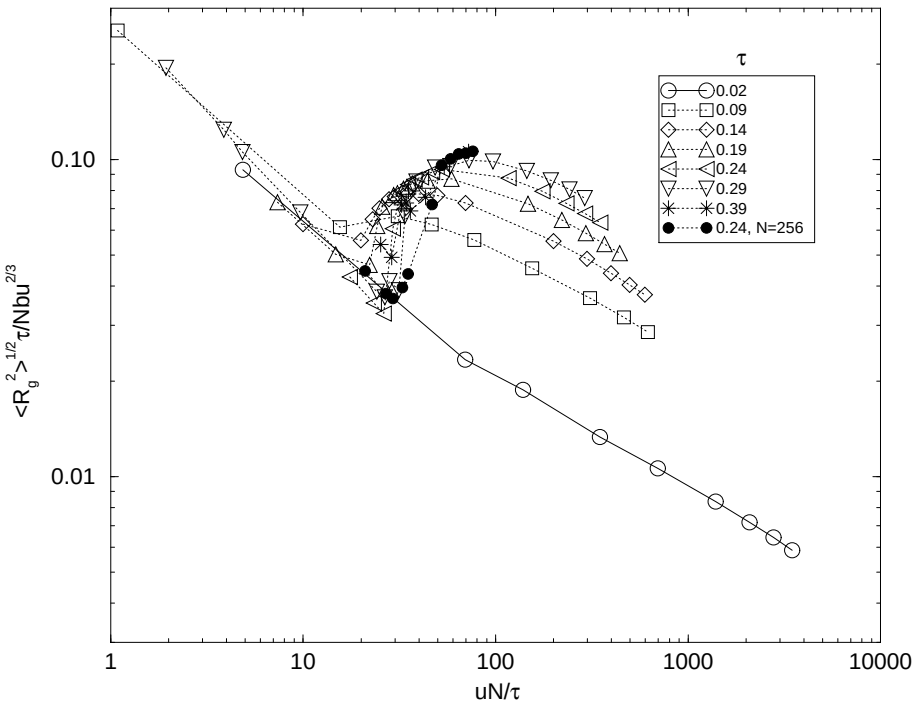

Figure 7: Reduced radius of gyration as a function of the parameter uN/τ. In each curve, τ is constant. The normalization is chosen such that the curves should be one constant for a) single–globule scaling, b) necklace scaling, and c) Khokhlov cylinder scaling. All data are for $N = 129$ except one curve as indicated.

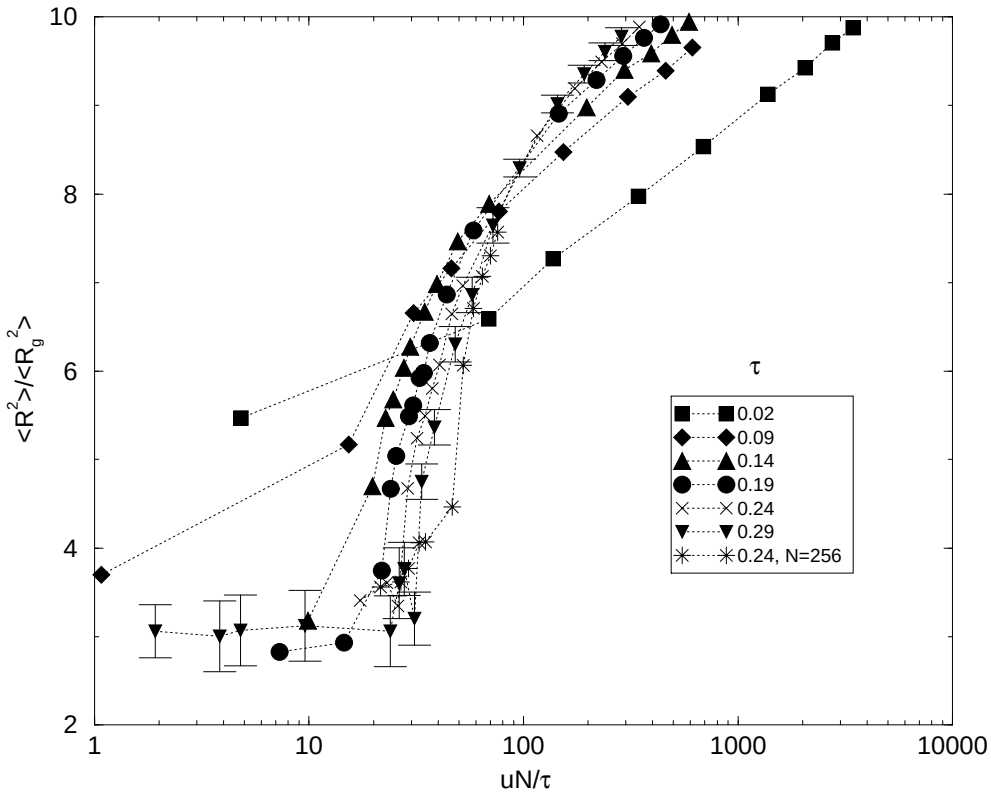

Figure 8: Ratio of the square end–to–end distance to the square of the gyration radius as a function of uN/τ for different values of τ and chain length $N = 129$ (except one curve as indicated).

(a)

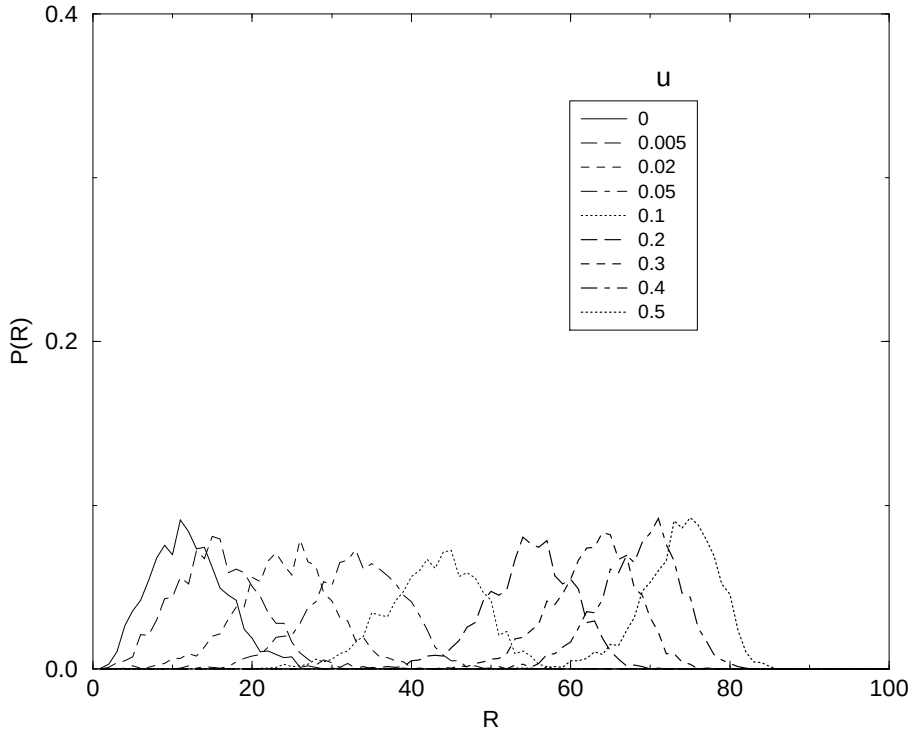
0.4
0.2
0.0
P(R)
0
20
40
60
80
100
R
u
0
0.005
0.02
0.05
0.1
0.2
0.3
0.4
0.5

(b)

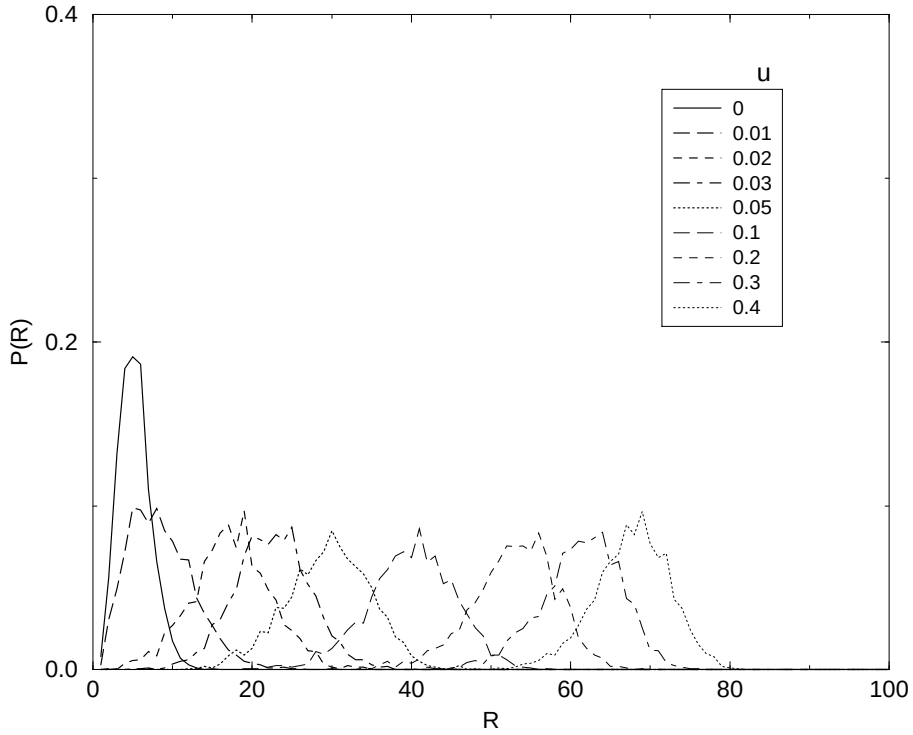
0.4
0.2
0.0
P(R)
0
20
40
60
80
100
R
u
0
0.01
0.02
0.03
0.05
0.1
0.2
0.3
0.4

(c)

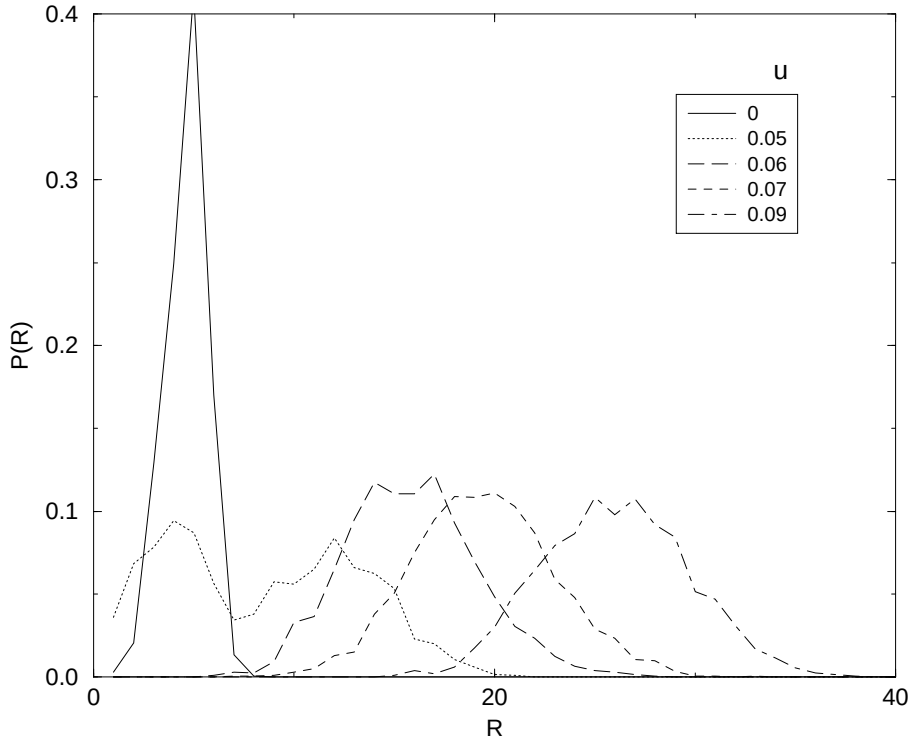

(d)

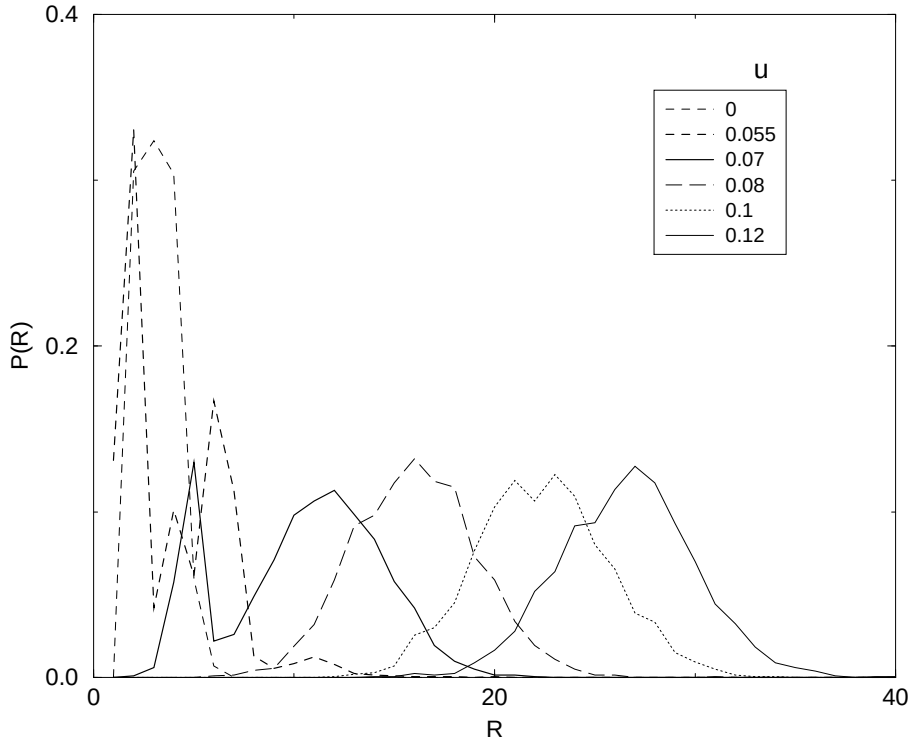

Figure 9: Probability distribution functions of the $N = 129$ chain end–to–end distance for different values of u: a) At the Θ point; b) $\tau = 0.09$; c) $\tau = 0.24$; d) $\tau = 0.29$.

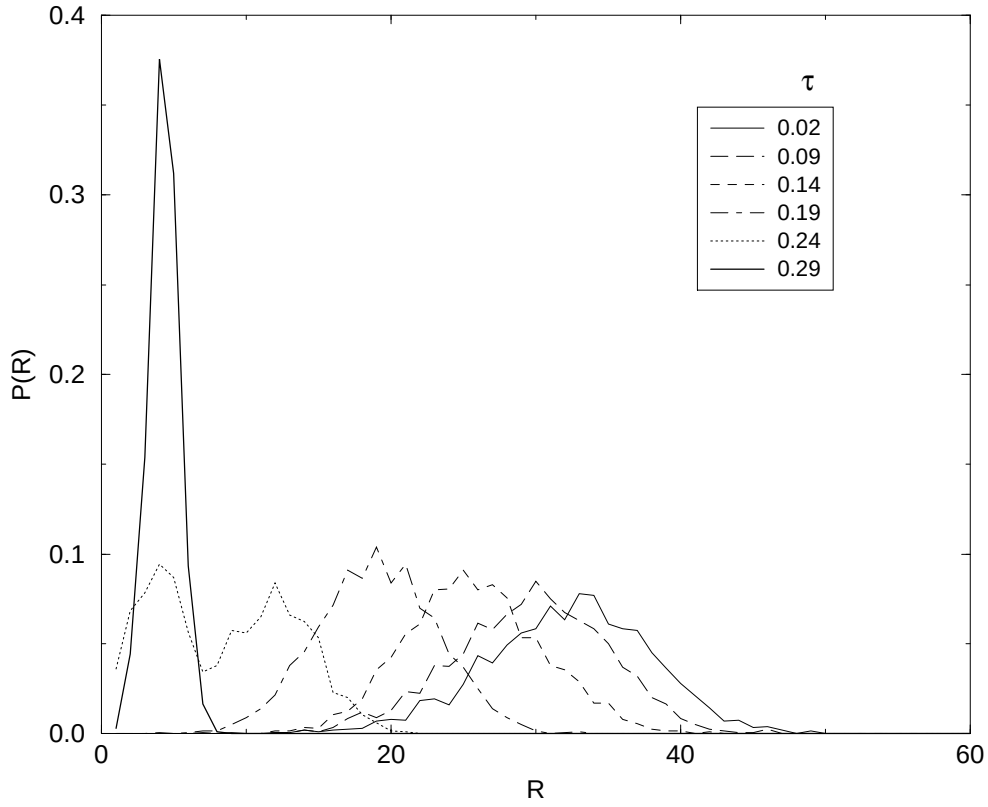

Figure 10: Distribution function of the chain end–to–end distance for $N = 129$ and different values of τ at $u = 0.05$.

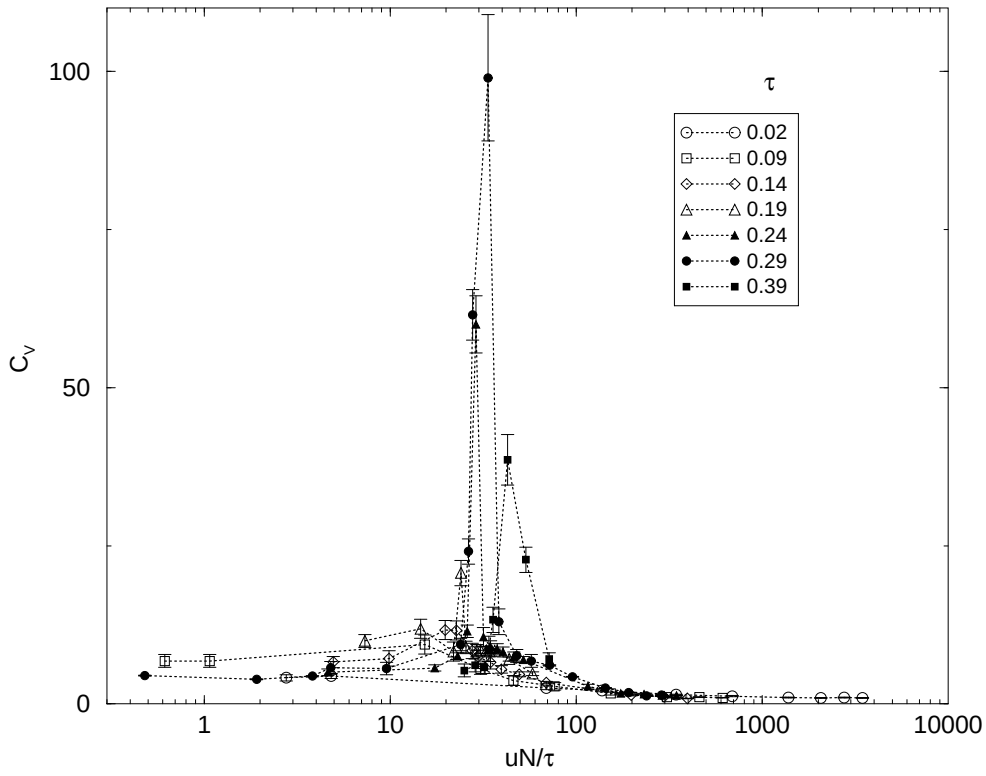

Figure 11: Specific heat per monomer as a function of uN/τ for different values of τ and chain length $N = 129$.

(a)

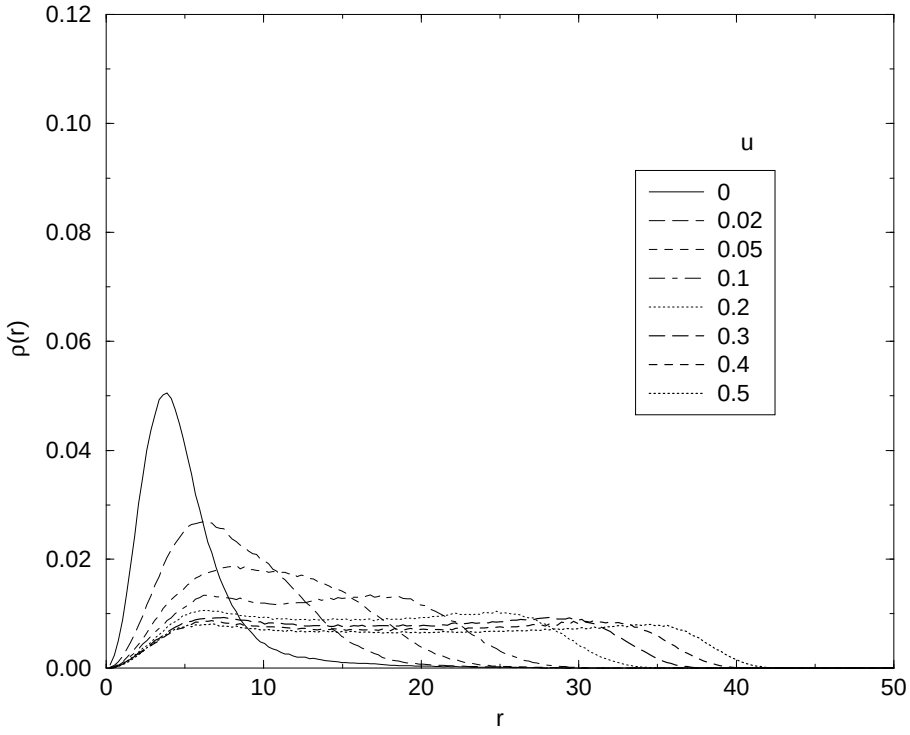

(b)

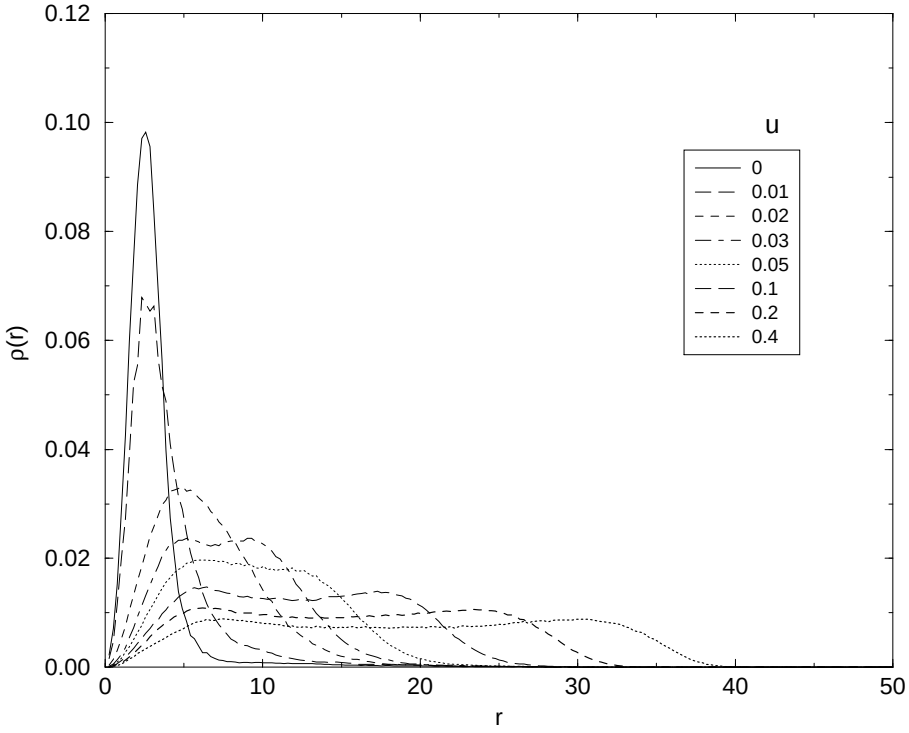
0.12
0.10
0.08
0.06
0.04
0.02
0.00
ρ(r)
0
10
20
30
40
50
r
u
0
0.01
0.02
0.03
0.05
0.1
0.2
0.4

(c)

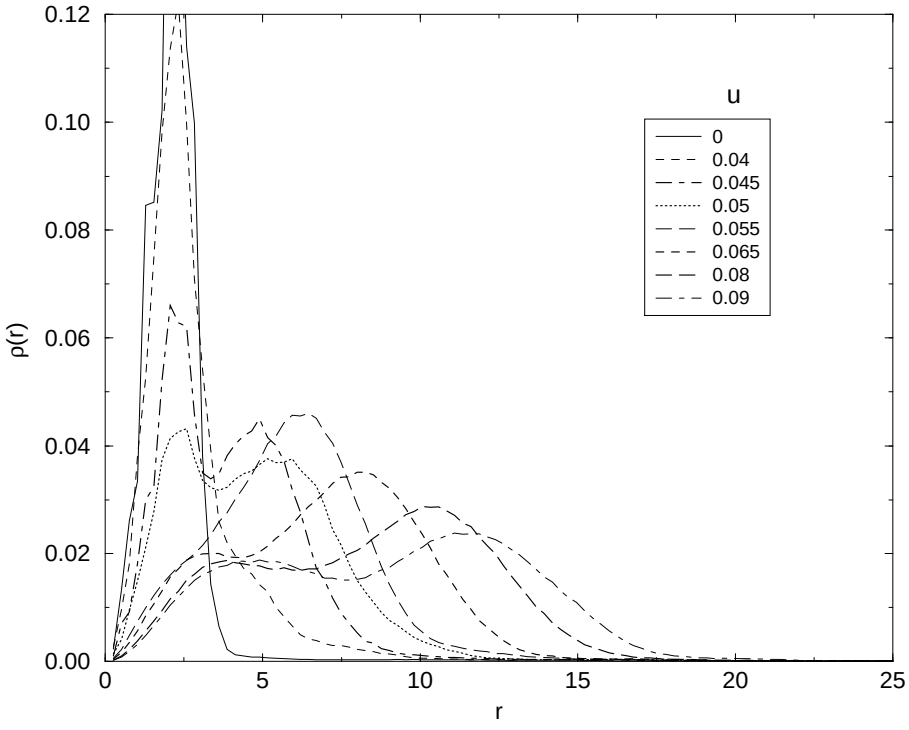
0.12
0.10
0.08
0.06
0.04
0.02
0.00
ρ(r)
0
5
10
15
20
25
r
u
0
0.04
0.045
0.05
0.055
0.065
0.08
0.09

(d)

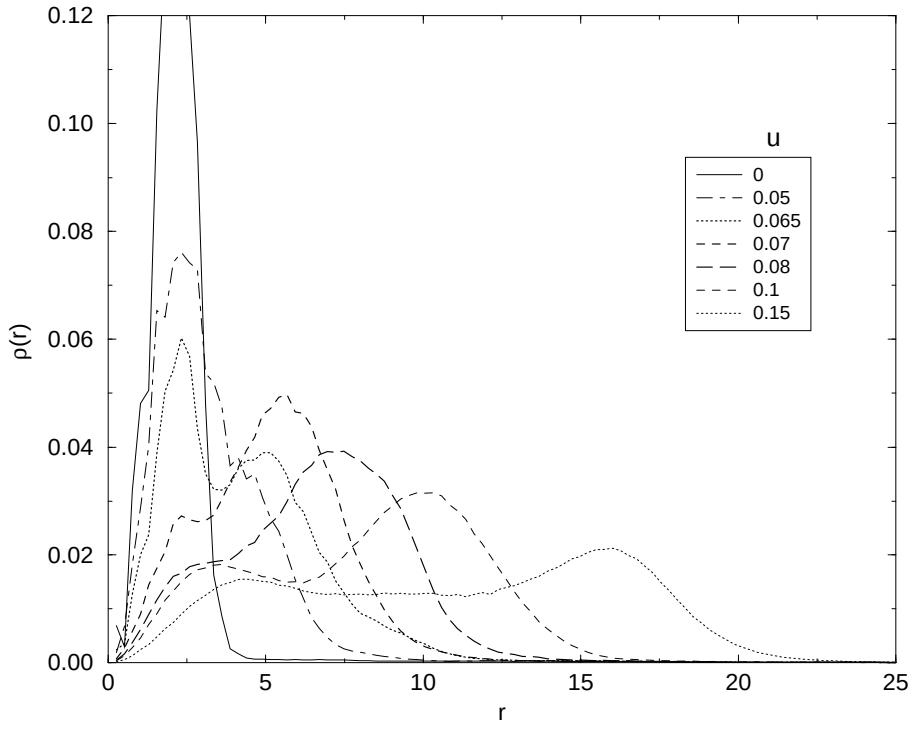

(e)

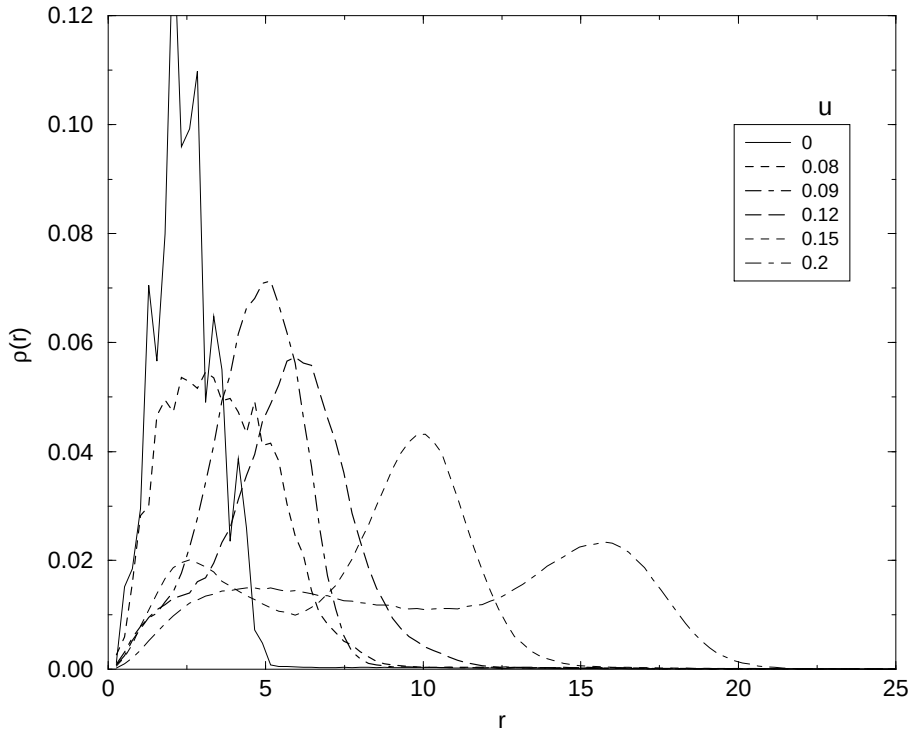

Figure 12: Density distribution function of monomers around the center of mass of a chain of $N = 129$ monomers, for different values of u: a) At the Θ point; b) $\tau = 0.09$; c) $\tau = 0.24$; d) $\tau = 0.29$ e) $\tau = 0.39$.

(a)

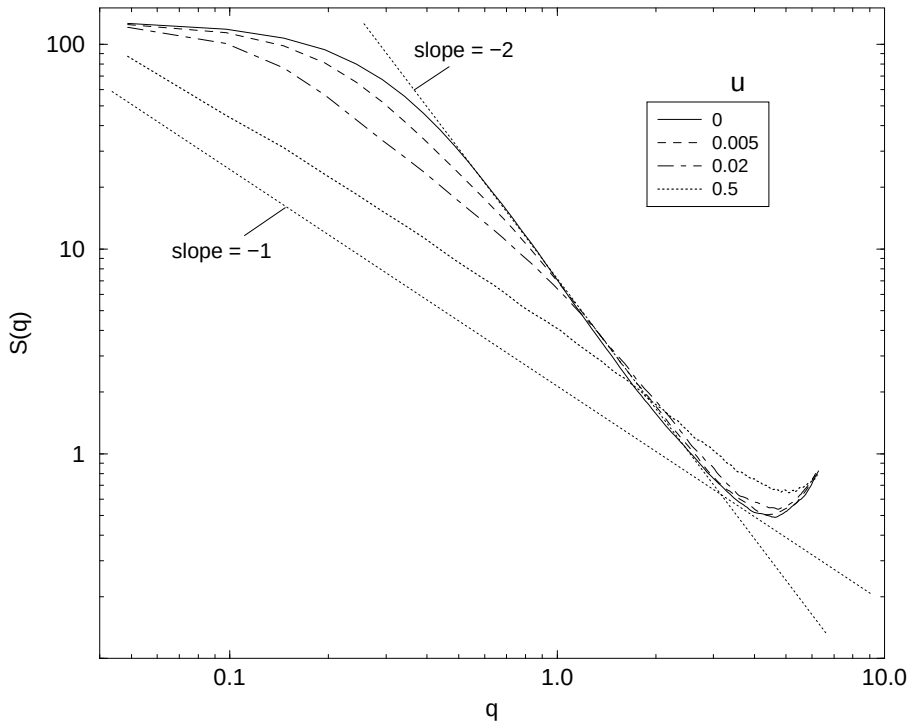
100
10
1
S(q)
0.1
1.0
10.0
q
slope = −2
slope = −1
u
0
0.005
0.02
0.5

(b)

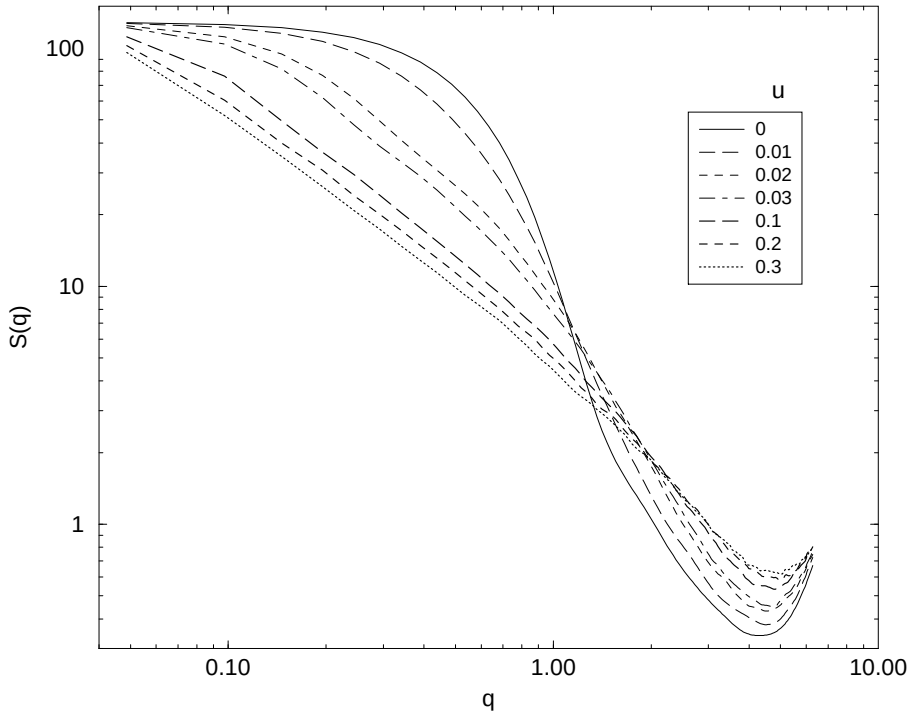
100
10
1
S(q)
0.10
1.00
10.00
q
u
0
0.01
0.02
0.03
0.1
0.2
0.3

(c)

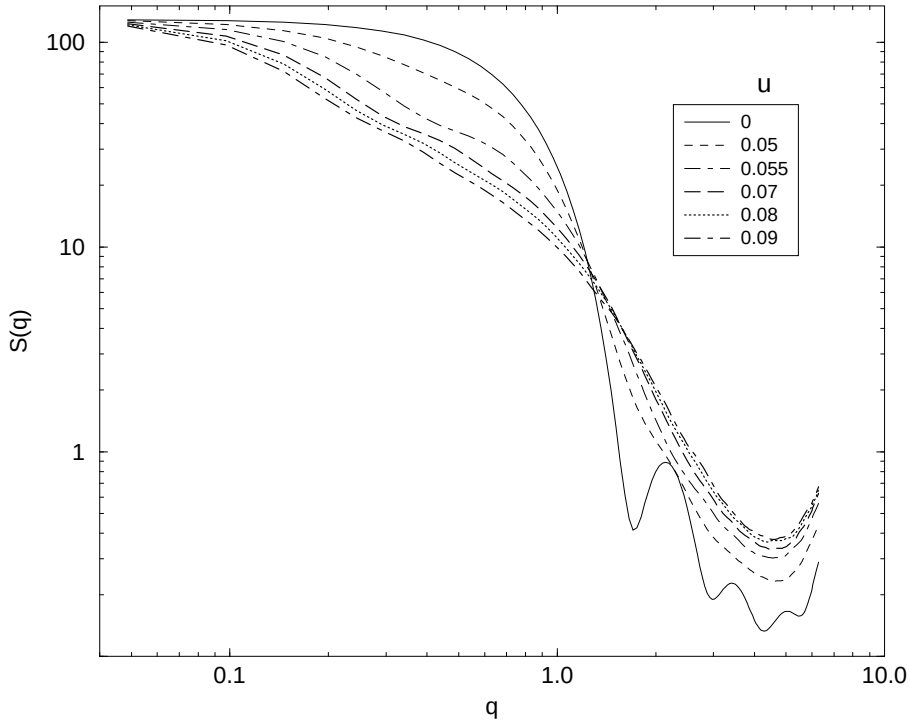
100
10
1
S(q)
0.1
1.0
10.0
q
u
0
0.05
0.055
0.07
0.08
0.09

(d)

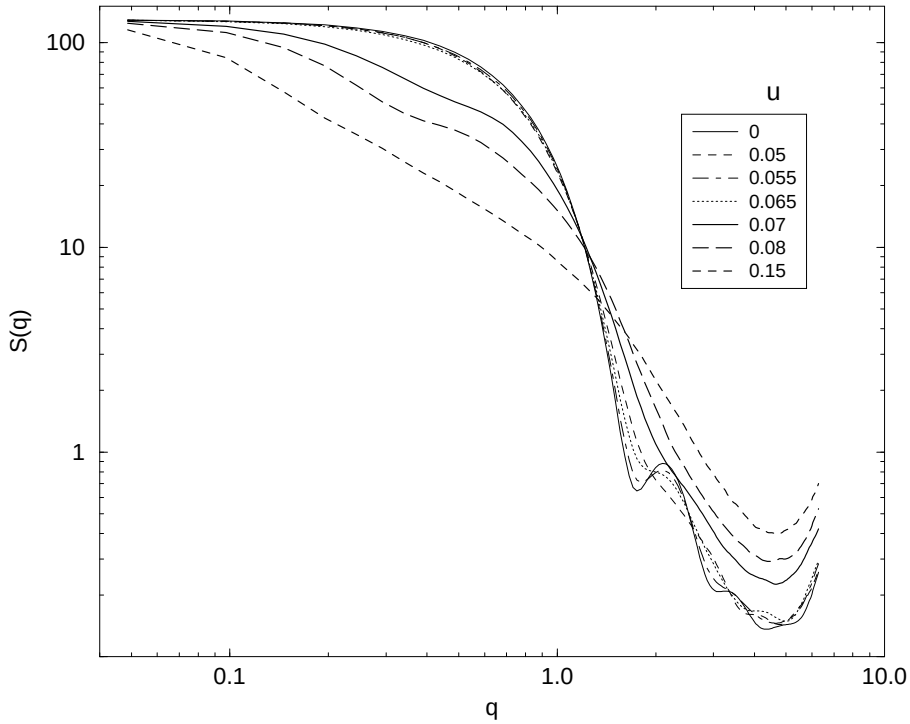
100
10
1
S(q)
0.1
1.0
10.0
q
u
0
0.05
0.055
0.065
0.07
0.08
0.15

(e)

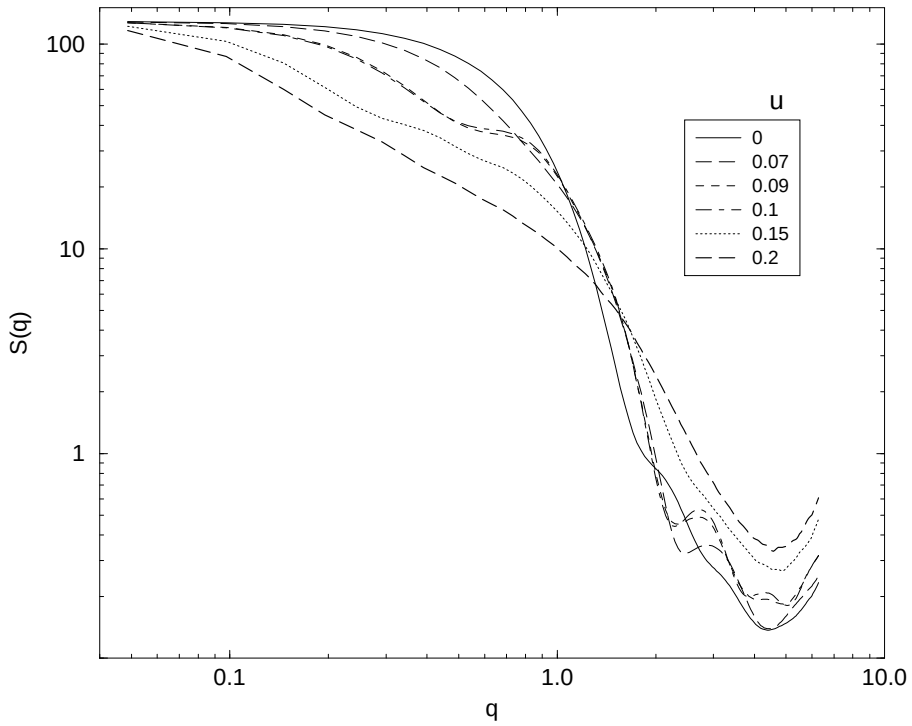

Figure 13: Spherically averaged structure factor of the $N = 129$ chain for different values of u: a) At the Θ point; b) $\tau = 0.09$; c) $\tau = 0.24$; d) $\tau = 0.29$; e) $\tau = 0.39$.

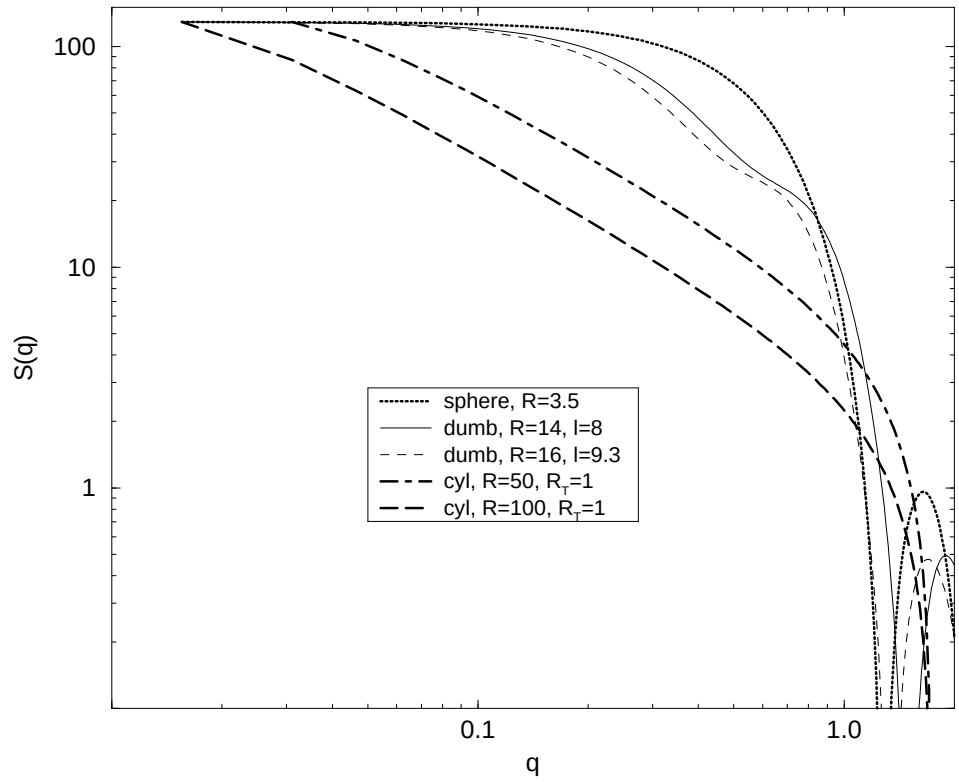

Figure 14: Structure factor for different model systems as indicated: Sphere with radius $R = 3.5$; dumbbell with total length $R = 14$ and string length $l = 8$; dumbbell with $R = 16$ and $l = 9.3$; cylinder with length $R = 50$ and thickness $R_T = 1$; cylinder with $R = 100$ and $R_T = 1$. The curves for the dumbbell were calculated using Eqn. 3.9.

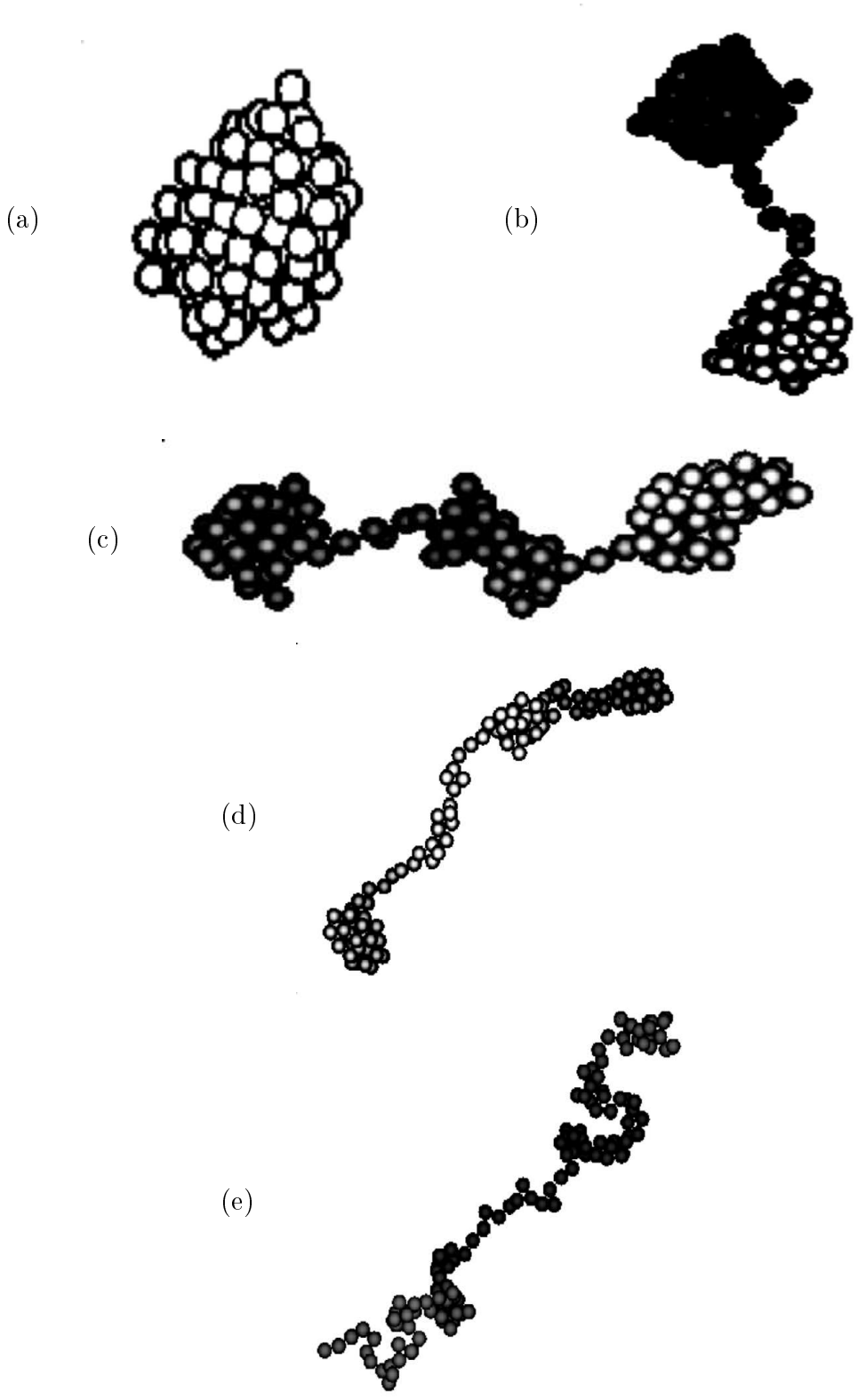

Figure 15: Snapshots of the conformations of the chain with $N = 129$ monomers at $\tau = 0.39$: a) Neutral chain, $u = 0$; b) $u = 0.1$; c) $u = 0.12$; d) $u = 0.15$; e) $u = 0.2$.